AD-A132 622 SIMULATION AND INTERPRETATION OF POLARIZATION DIVERSITY 1/
RADAR SPECTRAL FUNCTIONS(U) AIR FORCE GEOPHYSICS LAB
HANSCOM AFB MA J I METCALF 28 APR 83 AFGL-TR-83-0110

UNCLASSIFIED F/G 17/9 NL

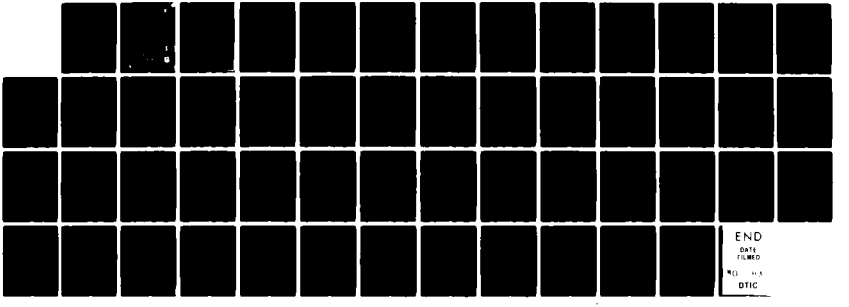

END
DATE FILMED
DTIC

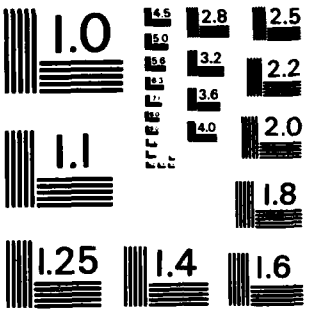

Simulation and Investigation of Polarization Diversity Radar Spectral Functions

JAMES I. METCALF

28 April 1983

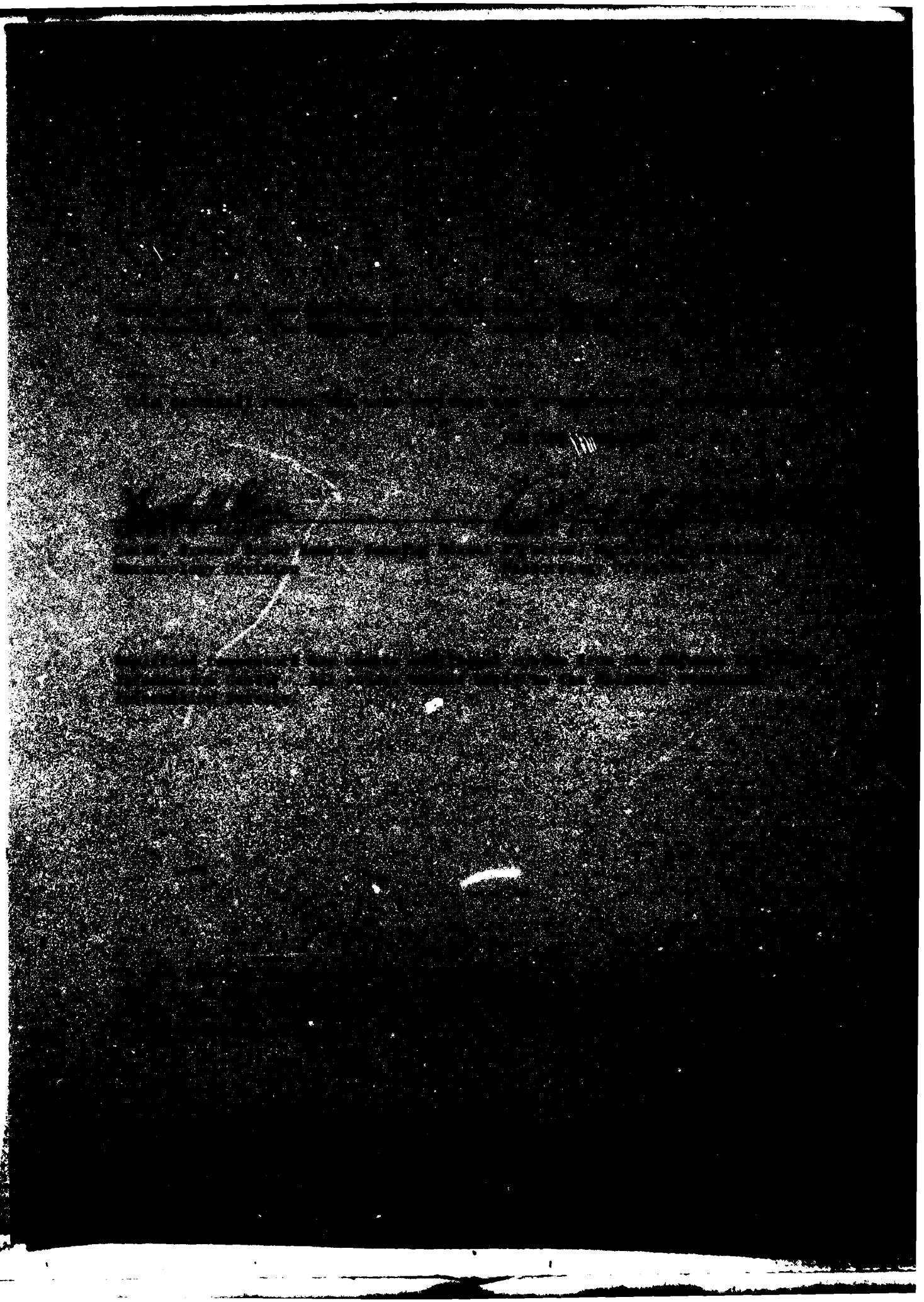

Unclassified

SECURITY CLASSIFICATION OF THIS PAGE (When Data Entered)

REPORT DOCUMENTATION PAGE		READ INSTRUCTIONS BEFORE COMPLETING FORM
1. REPORT NUMBER AFGL-TR-83-0110	2. GOVT ACCESSION NO.	3. RECIPIENT'S CATALOG NUMBER
4. TITLE (and Subtitle) SIMULATION AND INTERPRETATION OF POLARIZATION DIVERSITY RADAR SPECTRAL FUNCTIONS		5. TYPE OF REPORT & PERIOD COVERED Scientific. Interim. 6. PERFORMING ORG. REPORT NUMBER ERP, No. 835
7. AUTHOR(s) James I. Metcalf		8. CONTRACT OR GRANT NUMBER(s)
9. PERFORMING ORGANIZATION NAME AND ADDRESS Air Force Geophysics Laboratory (LYR) Hanscom AFB Massachusetts 01731		10. PROGRAM ELEMENT, PROJECT, TASK AREA & WORK UNIT NUMBERS 62101F 66701602
11. CONTROLLING OFFICE NAME AND ADDRESS Air Force Geophysics Laboratory (LYR) Hanscom AFB Massachusetts 01731		12. REPORT DATE 28 April 1983 13. NUMBER OF PAGES 52
14. MONITORING AGENCY NAME & ADDRESS(if different from Controlling Office)		15. SECURITY CLASS. (of this report) Unclassified 15a. DECLASSIFICATION/DOWNGRADING SCHEDULE

16. DISTRIBUTION STATEMENT (of this Report)

Approved for public release; distribution unlimited.

17. DISTRIBUTION STATEMENT (of the abstract entered in Block 20, if different from Report)

18. SUPPLEMENTARY NOTES

19. KEY WORDS (Continue on reverse side if necessary and identify by block number)

Radar meteorology
Polarization diversity radar
Radar signal analysis
Doppler radar
Coherent radar
Spectral analysis

20. ABSTRACT (Continue on reverse side if necessary and identify by block number)

A numerical model was developed to simulate the power spectra, cross-spectrum, and derived functions obtainable from a coherent polarization diversity radar. The model was used to investigate the effects of air velocity variance, differential propagation, and noise on the spectral functions. Input parameters include radar wavelength, elevation angle, air velocity variance, rainfall rate, propagation distance, fraction of scatterers having a preferred orientation, and relative noise level. Results of calculations for 8.6 mm and 7.5 cm wavelengths are illustrated. These are compared with the functional-

DD FORM 1 JAN 73 1473 EDITION OF 1 NOV 65 IS OBSOLETE

Unclassified

SECURITY CLASSIFICATION OF THIS PAGE (When Data Entered)

20. (Contd)

forms obtained from theory and discussed in terms of the meteorological information derivable from them. The forms of the spectral power ratio and the cross-spectral amplitude ratio are strongly affected by air velocity variance and by noise. However, it appears possible to derive a good estimate of the Doppler air velocity from the power spectra. The cross-spectral amplitude ratio may be of more general value in analysis than previously thought, because its Doppler velocity domain is greater than that of the spectral power ratio in the presence of radar systen noise. The absolute error of the propagation term estimated from the cross spectral amplitude ratio is not strongly dependent on the rainfall rate or propagation distance. However, it may be difficult to extract detailed quantitative backscatter information when significant propagation effects are present.

Contents

Illustrations

Tables

Simulation and Interpretation of Polarization Diversity Radar Spectral Functions

1. INTRODUCTION

The research described in the following sections is a continuation of the research reported by Metcalf and Echard[1] and Metcalf.[2,3] The earlier work documented various theoretical and practical aspects of the interpretation of signals receivable by coherent polarization-diversity radars, including the formulation of the received signals and the spectral functions derivable from them and the effects of propagation phenomena, non-Rayleigh scattering, variations in apparent or actual shape and orientation of hydrometeors, and air velocity variance on the received signals and spectral functions.

To elucidate these effects we developed numerical simulations of the spectral functions, following the approach of Warner and Rogers,[4] who computed power

(Received for publication 26 April 1983)

1. Metcalf, J.I., and Echard, J.D. (1978) Coherent polarization-diversity radar techniques in meteorology, J. Atmos. Sci. 35:2010-2019.
2. Metcalf, J.I. (1981) Propagation effects on a coherent polarization-diversity radar, Radio Sci. 16:1373-1383.
3. Metcalf, J.I. (1983) Interpretation of simulated polarization diversity radar spectral functions, Radio Sci. 18:in press.
4. Warner, C., and Rogers, R.R. (1977) Polarization-diversity Radar: Two Theoretical Studies, Sci. Reprt. MW-90, Stormy Weather Group, McGill University, Montreal, Quebec, Canada.

spectra corresponding to those which would be observed in the in the transmission channel (S_1) and orthogonal channel (S_2) of a 10-cm radar transmitting circular polarization. The present model yields the two power spectra and the cross-spectrum S_{12} of the two received signals. The latter function is of significance when there is either non-Rayleigh scattering or a non-negligible propagation effect, both of which are typically encountered at shorter radar wavelengths. The model development was originally conceived as a counterpart to empirical studies based on data from the 8.6-mm coherent polarization-diversity radar operated by the Wave Propagation Laboratory of the National Oceanic and Atmospheric Administration.[5] The simulation work also permitted us to develop and refine procedures for manipulating and displaying the spectral functions which could be used with spectral functions derived from radar data. This report documents the formulation of the model and presents a variety of computational results.

A similar set of model computations was presented by Metcalf and Matthews.[6] However, there were two errors in the model formulation used in that report which necessitated the publication of the present results. One error was in the computed magnitude of the propagation term, affecting computations for non-zero propagation distance. The other error was a misinterpretation of the scattering amplitude coefficients which resulted in an incorrect orientation of the scattering amplitude ratio in the complex plane. The computed cross-spectrum was thus in error in all cases and the power spectrum in the transmission channel (S_1) was in error in cases of non-zero propagation distance. Most of the qualitative conclusions of the previous report remain valid, but quantitative details differ, particularly in cases involving differential propagation effects. In addition to correcting the earlier results, the present report contains results of computations for 7.5 cm wavelength, corresponding to predominant Rayleigh scattering.

The results shown in Section 3 illustrate the effects of air velocity variance, noise, and differential propagation parameters on the spectral functions at a particular elevation angle and two rainfall rates. These results emphasize the requirement for low noise in the received signals, so that the spectral power ratio S_1/S_2 and the cross-spectral amplitude ratio S_{12}/S_2 can provide useful information on backscatter characteristics across the Doppler velocity domain. The presence of noise precludes the measurement of either of these ratios at very low Doppler velocities where propagation effects, if present, would first dominate backscattering

5. Pasqualucci, F., Bartram, B.W., Kropfli, R.A., and Moninger, W.R. (1983) A millimeter-wavelength dual-polarization Doppler radar for cloud and precipitation studies, J. Clim. Appl. Meteor. 22:758-765.

6. Metcalf, J.I., and Matthews, J.E., III (1981) Numerical Simulation of Coherent Polarization-diversity Radar Spectral Functions, Scientific Report No. 1, Natl. Sci. Foundation Grant ATM-8018382, Project A2818, Engr. Expt. Stn., Ga. Inst. of Tech., Atlanta, Georgia.

effects. Hence the separation of propagation and backscattering effects, as postulated by Metcalf,[2] will prove to be a more complicated process than initially envisioned. With increasing air velocity variance, the numerical characteristics of the spectral functions at all velocities tend to approach the characteristics of the corresponding integrated quantities. Since the first maximum and minimum of the Mie scatter cross-section occur at relatively large drop sizes at 8.6 mm radar wavelength, the spectral features associated with these extrema occur at Doppler velocities well above those of the spectral peaks; with increasing air velocity variance, these features appear at relatively higher Doppler velocities. Therefore, in the interpretation of spectra computed from experimental data, it will be necessary to make an adjustment for air velocity variance before particular features of the spectral functions can be identified with particular Doppler fall speed components.

2. NUMERICAL CONCEPTS

2.1 Spectral Function Formulations

The power spectra derived from signals in the transmission channel (S_1) and the orthogonal channel (S_2) and the cross-spectrum (S_{12}) of the two received signals can be expressed as

$$S_1(v) = \int_0^\infty \sigma(r,\phi)\, G(V(r)\sin\phi, \Sigma)\, N(r) \times \left| \nu(r,\phi)\, e^{j[\delta(r,\phi) \pm 2\alpha(r,\phi)]} + 2p\, e^{j(\lambda \pm 2\tau)} \right|^2 dr \quad (1)$$

$$S_2(v) \int_0^\infty \sigma(r,\phi)\, G(V(r)\sin\phi, \Sigma)\, N(r)\, dr \quad (2)$$

$$S_{12}(v) = \int_0^\infty \sigma(r,\phi)\, G(V(r)\sin\phi, \Sigma)\, N(r) \times \left(\nu(r,\phi)\, e^{j[\delta(r,\phi) \pm 2\alpha(r,\phi)]} + 2p\, e^{j(\lambda \pm 2\tau)} \right) dr \quad (3)$$

where v is the Doppler velocity defined as positive toward the radar, σ is the backscatter cross-section, r is the equivalent spherical radius of a drop, ϕ is the elevation angle, N(r) is the drop size distribution function, and α is the orientation angle or canting angle of each scatterer. The velocity weighting function is defined by

$$G(V(r)\sin\phi, \Sigma) = \frac{1}{\Sigma\sqrt{2\pi}} \exp\left(- \frac{(v - V(r)\sin\phi)^2}{2\Sigma^2} \right) \quad (4)$$

where $V(r)$ is the raindrop fall speed in calm air and Σ^2 is the Doppler velocity variance due to turbulence or wind shear. One could include a non-zero mean wind by substituting $[V(r)\sin\phi + V_a]$ for $[V(r)\sin\phi]$ in Eq. (4), where V_a is the radial component of the air velocity. The complex backscatter amplitude ratio is defined for a spheroidal hydrometeor by

$$\nu(r, \phi)\, e^{j\delta(r,\phi)} = \frac{S_{xx}(r, \phi) - S_{yy}(r, \phi)}{S_{xx}(r, \phi) + S_{yy}(r, \phi)} \quad (5)$$

where S_{xx} and S_{yy} are the backscatter amplitude coefficients for signals of polarizations parallel and perpendicular, respectively, to the symmetry axis of the spheroid. For Rayleigh scattering from oblate spheroids, $S_{yy} > S_{xx}$, and the amplitude ratio lies near the negative real axis. This condition can be described either by $\nu < 0$ and $\delta \approx 0$ or by $\nu > 0$ and $\delta \approx \pi$. We use the latter convention. The propagation term $\rho e^{j(\chi + \tau)}$ is based on a model of an anisotropic (precipitation filled) medium with symmetry axes rotated through an angle τ from the vertical and horizontal. The other propagation parameters are related to the total one-way differential attenuation ΔA and differential phase shift $\Delta\Phi$ in the medium to first-order approximation by

$$\rho e^{j\chi} = \tanh(0.05756\, \Delta A + j(\pi/360)\, \Delta\Phi) . \quad (6)$$

The upper and lower signs in Eqs. (1) and (2) and elsewhere correspond to the transmission of right and left circular polarization, respectively.

The spectrum defined in Eq. (2) yields the relation

$$\eta = \int_{-\infty}^{\infty} S_2(v)\, dv \quad (7)$$

where η is the reflectivity in units of inverse length, that is, cross-section per unit volume. The backscatter cross-section is given by

$$\sigma = \pi\, |S_{xx}(r, \phi) + S_{yy}(r, \phi)|^2 . \quad (8)$$

For our computations, we used values of S_{xx} and S_{yy} computed by Oguchi and Hosoya.[7] These computations were based on the linear size-shape relation of Spilhaus,[8] rather than the more realistic Pruppacher and Pitter[9] size-shape relation, and our results therefore cannot be strictly representative of what one might observe in nature.

Warner and Rogers[4] computed power spectra up to proportionality for Rayleigh scattering from raindrops having shapes as described by Pruppacher and Pitter. Their computations included air velocity standard deviation, radar elevation angle, rainfall rate, and fraction of preferentially oriented scatterers as computational parameters. The elevation angle affects the relative significance of fall speed variance and air velocity variance, and the rainfall rate affects the drop size distribution through the assumed Marshall and Palmer[10] distribution function. We included all these parameters in our model and added propagation distance as a parameter to simulate non-negligible differential propagation effects.

The functions of greatest interest are the power spectrum S_2 (in the channel opposite to the transmission channel), the spectral power ratio S_1/S_2, the normalized cross-spectrum $S_{12}/(S_1S_2)^{1/2}$, and the function S_{12}/S_2 which is of particular interest where propagation effects are present. The functions S_1/S_2 and S_{12}/S_2 are essentially weighted averages of the squared absolute value in Eq. (1) and the quantity in brackets in Eq. (3), respectively, and can be expressed as

$$S_1/S_2 = \overline{r^2} + 4p^2 + 4\,\mathrm{Re}\left(p e^{-j(\lambda + 2\tau)}\, \overline{r e^{j(\delta + 2\alpha)}} \right) \tag{9}$$

$$S_{12}/S_2 = \overline{r\, e^{j(\delta + 2\alpha)}} + 2p\, e^{j(\lambda + 2\tau)}. \tag{10}$$

where the overbars indicate integration over drop size, as shown explicitly in Eqs. (1), (2), and (3). Because the function S_{12}/S_2 contains the backscatter amplitude ratio r and the propagation parameter p, which is also an amplitude ratio, we suggest that this function be called the "cross-spectral amplitude ratio." (The comparable parameter for non-coherent radar, W/W_2 in the notation of McCormick and Hendry,[11] can be called the "cross-covariance amplitude ratio.") The normalized cross-spectrum, the magnitude of which is the coherency, is related to the two functions above by

$$S_{12}/(S_1S_2)^{1/2} = \frac{S_{12}/S_2}{(S_1/S_2)^{1/2}}. \tag{11}$$

(Due to the large number of references cited above, they will not be listed here. See References, page 51.)

For modeling of the spectral functions, it is useful to express the averaged quantities in terms of parameters that allow some separation of variables and that characterize both the extent to which the medium is preferentially oriented and the orientation angle. Ultimately, it will be necessary to include the effect of shape variation on the backscatter power and amplitude ratios. The following subsections discuss in more detail the formulation of these ratios in the model.

2.2 Backscatter Amplitude Ratio

The backscatter amplitude ratio defined in Eq. (5) is shown in Figure 1 for two wavelengths and two elevation angles, based on the Oguchi and Hosoya amplitude coefficients. Comparing the curves for the two elevation angles at each wavelength, one can verify that the magnitude of the ratio is approximately proportional to $\cos^2\phi$ and that the phase angle δ is not strongly dependent on the elevation angle, except for drop diameters near half the wavelength, that is, between 4.0 and 4.5 mm diameter for 8.6-mm wavelength.

To evaluate the term $\overline{\nu\, e^{j(\delta \pm 2\alpha)}}$ for a collection of raindrops we use the approach of McCormick and Hendry.[11] We assume that drops of a given radius have a distribution of canting angles and integrate the quantity $\nu_i(r,\phi)\exp[j(\delta_i(r,\phi) \pm 2\alpha_i(r,\phi))]$, corresponding to an individual drop, over all orientations to obtain the result

$$\nu\, e^{j(\delta \pm 2\alpha)} = \rho_{\alpha}(r,\phi)\ \nu_i(r,\phi)\, e^{j(\delta_i(r,\phi) \pm 2\bar{\alpha}(r,\phi))} \tag{12}$$

where

$$\rho_{\alpha}(r,\phi) = \int_{\bar{\alpha}-\pi/2}^{\bar{\alpha}+\pi/2} \cos\left[2(\alpha-\bar{\alpha})\right]\ T(\alpha-\bar{\alpha})\ d(\alpha-\bar{\alpha}) \tag{13}$$

$\bar{\alpha}$ is the average orientation angle, and $T(\alpha-\bar{\alpha})$ is the symmetrical distribution of canting angles. This result is equivalent to that corresponding to a medium having a fraction ρ_{α} of scatterers with a fixed orientation angle $\bar{\alpha}$ and a fraction $1-\rho_{\alpha}$ with a uniform random distribution of orientation angles. If ρ_{α} and $\bar{\alpha}$ are independent of drop size, they can be factored out of the right side of Eq. (12). The quantities $\bar{\nu}$ and $\bar{\delta}$ can then be defined as functions of Doppler velocity by

$$\bar{\nu}\, e^{j\bar{\delta}} = \frac{\int_0^{\infty} \sigma(r,\phi)\, N(r)\, G\, \nu(r,\phi)\ e^{j\delta(r,\phi)}\, dr}{\int_0^{\infty} \sigma(r,\phi)\, N(r)\, G\, dr}. \tag{14}$$

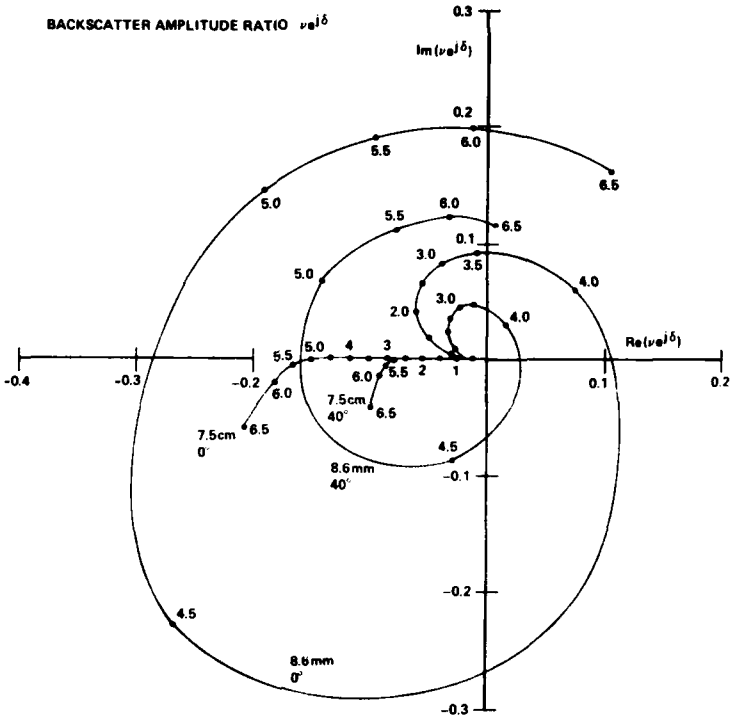

Figure 1. Backscatter amplitude ratio $\nu e^{j\delta}$ for raindrops, incorporating the Spilhaus size-shape relation and based on the scattering coefficients calculated by Oguchi and Hosoya. Calculations are shown for 0.5 mm increments of equivalent spherical diameter for wavelengths of 7.5 cm and 8.6 mm and elevation angles of 0° and 40°. Rayleigh scattering approximation holds for D < 5 mm at 7.5 cm wavelength and for D < 0.6 mm at 8.6 mm. Magnitude of ratio is approximately proportional to $\cos^2 \phi$. Dependence of the phase shift δ on elevation angle is negligible for Rayleigh scattering but significant for drops with D/λ near 0.5.

If the weighting function G is omitted from the integrals, then the definition applies to the entire array of hydrometeors. The use of $\bar{\nu}$ and $\bar{\delta}$ as separate parameters is of uncertain value, as the two cannot easily be modeled separately, except in the case of Rayleigh scattering where $\bar{\delta} \simeq 0$ or π. One can, however, approximately separate the size and elevation angle dependences of the quantities in Eq. (12), since δ is approximately independent of elevation angle and $\nu_i(r, \phi) \simeq \nu_i(r, 0) \cos^2 \phi$ where $\nu_i(r, 0)$ is the amplitude ratio for a drop viewed perpendicular to its axis of rotational symmetry, that is, horizontally.

In summary, the backscatter amplitude ratio for a collection of scatterers results only from those scatterers having a common orientation. The amplitude ratio for those scatterers can be computed either from the scattering amplitude coefficients for the specified radar elevation angle or (approximately) from the scattering amplitude coefficients for zero elevation angle. We use the former procedure in our computations

2.3 Backscatter Power Ratio

We follow the approach of Warner and Rogers[4] in formulating the backscatter power ratio. This quantity is the sum of two terms, corresponding to the preferentially oriented fraction ρ_α and the randomly oriented fraction $(1-\rho_\alpha)$, respectively. The power ratio can be expressed as

$$\nu^2(r,\phi) = \left(\rho_\alpha(r)\cos^4\phi + [1-\rho_\alpha(r)](8/15)\right)\nu_i^2(r,0) \qquad (15)$$

where $\nu_i^2(r,0)$ is the backscatter power ratio for a drop viewed at horizontal incidence and the relation $\nu_i(r,\phi) = \nu_i(r,0)\cos^2\phi$ is assumed. The factor 8/15 results from integrating $\cos^4\phi$ over all orientations. Alternately, we can calculate the quantity $\nu_i^2(r,\phi)$ directly from the scattering amplitude coefficients. Using this procedure, we compute the power ratio by the formula

$$\nu^2(r,\phi) = \rho_\alpha(r)\nu_i^2(r,\phi) + [1-\rho_\alpha(r)]\ (8/15)\ \nu_i^2(r,0) \qquad (16)$$

The power ratio $\nu_i^2(r,0)$ calculated from the scattering amplitude coefficients of Oguchi and Hosoya is shown in Figure 2 for two wavelengths as a function of fall speed V(r) which was calculated from the formula of Best.[12] While one could not obtain this curve from actual observations at zero elevation angle, because the Doppler velocity component due to fall speed is proportional to $\sin\phi$, one could obtain an approximation to the curve by plotting $(S_1/S_2)/\cos^4\phi$ against $v/\sin\phi$. The result would be identical to Figure 2 in the ideal case of a completely oriented medium with zero air velocity. Non-zero air velocity would result in a displacement along the abscissa. Propagation effects and air velocity variance result in changes which are discussed and illustrated in Section 3.

---

12. Best, A.C. (1950) Empirical formulae for the terminal velocity of water drops falling through the atmosphere, Quart. J. Roy. Meteor. Soc. 76:302-311.

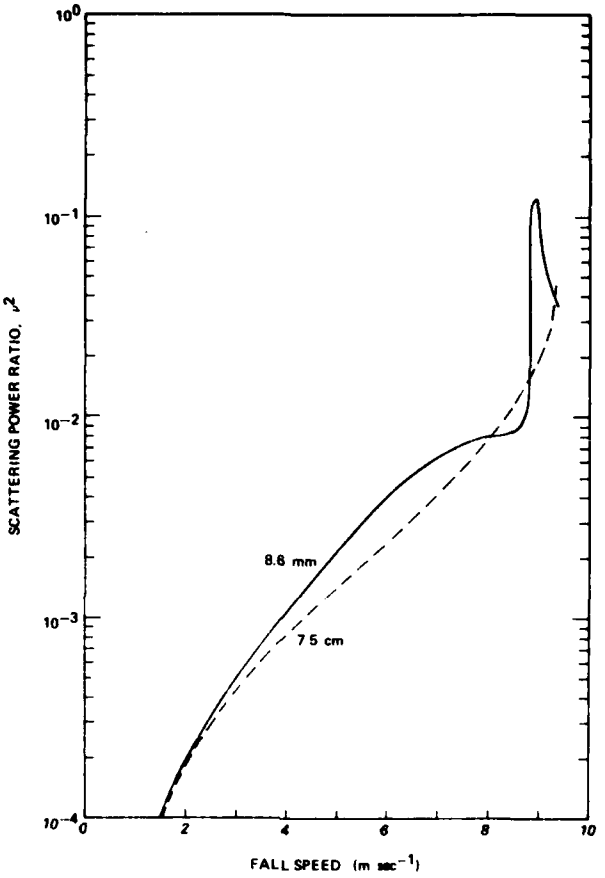

Figure 2. Scattering power ratio at zero elevation angle as a function of raindrop fall speed for radar wavelengths of 7.5 cm and 8.6 mm, based on the calculations shown in Figure 1. Power ratio for 8.6 mm shows sharp increase near 8.8 m sec^{-1} fall speed, corresponding to drops of diameter near half the wavelength.

The foregoing results allow the spectral functions to be expressed in terms of the subsidiary functions $\overline{\nu^2}(v)$, $\nu(v)$, and $\overline{\delta}(v)$, so that Eqs. (9) and (10) become

$$S_1/S_2 = \overline{\nu^2}(v) + 4p^2 + 4\rho_\alpha \, \mathrm{Re}[p e^{j(\chi \pm 2\tau)} \, \overline{\nu}(v) \, e^{j(\overline{\delta}(v) \pm 2\overline{\alpha})}] \tag{17}$$

$$S_{12}/S_2 = \rho_\alpha \, \overline{\nu}(v) \, e^{j(\overline{\delta}(v) \pm 2\overline{\alpha})} + 2p e^{j(\chi \pm 2\tau)} . \tag{18}$$

2.4 Computational Parameters and Procedures

Our model requires as input parameters the rainfall rate, air velocity standard deviation Σ, radar elevation angle ϕ, preferential orientation factor ρ_α, and propagation distance. We use the scattering amplitude coefficients and rates of differential attenuation (dB km^{-1}) and differential phase shift (deg km^{-1}) from Oguchi and Hosoya. Consequently the model computations are restricted to the frequencies (4, 6, 11, 19.3, 30, and 34.8 GHz) and the elevation angles (0°, 20°, 40°, and 60°) for which the amplitude coefficients were calculated and the rainfall rates for which ΔA and $\Delta\Phi$ were calculated (0.25, 1.25, 2.5, 12.5, 25, 50, 100, and 150 mm hr^{-1}). We use the Marshall and Palmer raindrop size distribution function and the fall speed formula of Best. For simplicity we assume $\bar{\alpha} = \tau = 0$.

We calculate the term $p e^{j\chi}$ for the specified propagation distance. We then calculate three integral quantities at intervals of 0.1 m sec^{-1} between -2 and 16 m sec^{-1}:

$$I_1(v) = \int_{r_{min}}^{r_{max}} \sigma(r,\phi)\, N(r)\, G(V(r)\sin\phi,\ \Sigma)\, dr \tag{19}$$

$$I_2(v) = \int_{r_{min}}^{r_{max}} \sigma(r,\phi)\, N(r)\, G(V(r)\sin\phi,\ \Sigma) \times \left(\rho_\alpha \nu_i^2(r,\phi) + (1-\rho_\alpha)\,\frac{8}{15}\,\nu_i^2(r,0)\right) dr \tag{20}$$

$$I_3(v) = \rho_\alpha \int_{r_{min}}^{r_{max}} \sigma(r,\phi)\, N(r)\, G(V(r)\sin\phi,\ \Sigma)\, \nu_i(r,\phi)\, e^{j\delta_i(r,\phi)}\, dr\,. \tag{21}$$

We use $r_{min} = 0.1$ mm, $r_{max} = 3.25$ mm, and $\Delta r = 3.15 \times 10^{-3}$ mm, interpolating the scattering coefficients linearly between the radii at which they were calculated.

The power spectra and cross-spectrum are then calculated as follows:

$$S_1(v) = I_2(v) + 4p^2 I_1(v) + 4\,\mathrm{Re}\,[p e^{-j\chi} I_3(v)] \tag{22}$$

$$S_2(v) \equiv I_1(v) \tag{23}$$

$$S_{12}(v) = I_3(v) + 2p e^{j\chi} I_1(v)\,. \tag{24}$$

From these we form the secondary spectral functions S_1/S_2 and S_{12}/S_2. We integrate the three primary spectral functions to obtain an approximation of the total reflectivity as defined in Eq. (8), the circular depolarization ratio, the cross-covariance and cross-correlation, and the Doppler velocity mean and standard deviation in each channel.

Noise in the spectral functions can be simulated in two ways. Receiver noise is simulated by adding to both power spectra a uniform noise spectral density at a specified decibel level below the peak of the spectrum S_2. This corresponds to radar system noise with a Delta function autocorrelation and zero cross-correlation between the noise and the signal. Because this noise in either channel is assumed to be uncorrelated with the signal and with the noise in the other channel, it has no effect on the cross-spectrum. Noise due to spectral leakage, as would be encountered in spectrum analysis procedures applied to experimental data, is simulated by adding to each function a uniform noise spectral density at a specified decibel level below the peak magnitude of that function. In the case of the cross-spectrum, the constant is complex and has the same argument (or phase) as the peak of the cross-spectrum. In the analysis of experimental data the noise spectral density is likely to be dominated more often by spectral leakage than by receiver noise. The most common situation, however, is likely to combine the effects of spectral leakage with radar system noise which is correlated between the two channels due to its origin, for example, in a local oscillator.

The computations illustrated in the following section were performed at Air Force Geophysics Laboratory on a Perkin-Elmer 3242 computer and the results were plotted by a California Computer Products CALCOMP 1055 plotter. Some apparently anomalous features of the plotted functions are due to the numerical limits of the computer, that is, at the edges of the Doppler velocity domain of the functions. Numerical accuracy of the results is also affected by the procedures we used, including the trapezoid-rule integration, the radius limits, and the linear interpolation of the scattering coefficients.

3. RESULTS

The initial objective of the numerical simulation was to duplicate the theoretical forms of the amplitude and power ratios (Figures 1 and 2), determining the values of the computational parameters for which this can best be done and the ways in which changes in computational parameters affect the forms of the output. Computations were performed for 40° elevation angle, 2.5 and 25 mm hr^{-1} rainfall rates, and several values of air velocity variance, propagation distance, and noise. This elevation angle was chosen to yield the best compromise between variance due to

Doppler fall speed, varying as $\sin^2\phi$, and backscatter amplitude ratio, varying as $\cos^2\phi$. Most of the calculations were done for 8.6 mm wavelength.

Some of the integrated parameters are shown in Table 1. The circular depolarization ratio (CDR) and Doppler mean velocities are smaller for the lower rainfall rate, due to the greater proportion of smaller, more spherical drops. Differential attenuation and differential phase shift are of comparable importance at this wavelength, as is evident in the vector change of the cross-covariance amplitude ratio (CCAR) with propagation distance. Because of the relative phases of the scattering and propagation terms, the initial effect of propagation is to decrease the magnitude of the spectrum S_1, especially at the low-velocity end. Hence at short propagation distances the CDR decreases and the velocity $\bar{v}_1$ increases. At greater propagation distances, the CDR increases and the velocity $\bar{v}_1$ asymptotically approaches $\bar{v}_2$. The asymptotic behavior is more rapid at 25 mm hr^{-1} rainfall rate because of the larger differential attenuation and phase shift.

Table 1. Circular Depolarization Ratio (CDR), Cross-Covariance Amplitude Ratio (CCAR), and Doppler Mean Velocities as Functions of Rainfall Rate (R) and Propagation Distance (d), for 8.6 mm Wavelength and 40° Elevation Angle

R	d	CDR	CCAR			$\bar{v}_1$	$\bar{v}_2$
(mm hr^{-1})	(km)	(dB)	magnitude (absolute)	(dB)	phase (deg)	(m sec^{-1})	(m sec^{-1})
2.5	0	-28.80	0.0342	-14.66	147.0	4.06	3.70
	0.5	-28.93	0.0337	-14.73	140.7	4.09	
	1.0	-28.97	0.0335	-14.75	134.3	4.12	
	2.0	-28.75	0.0345	-14.62	121.7	4.14	
	4.0	-27.44	0.0407	-13.90	100.6	4.09	
25	0	-27.50	0.0396	-14.02	137.0	4.51	4.26
	0.5	-27.55	0.0393	-14.05	80.5	4.64	
	1.0	-23.44	0.0657	-11.83	50.3	4.46	
	2.0	-17.36	0.135	-8.70	33.3	4.33	

The following subsections discuss the effects of turbulence, differential propagation, and noise in more detail. Attention is placed primarily on the possibilities of separating Doppler velocity components due to air velocity and fall speed, separating scattering and propagation effects, and interpreting the spectral functions in

the presence of noise. The final subsection discusses and illustrates these effects in relation to Rayleigh scattering.

3.1 Turbulence Effects

Computations for scattering at 8.6 mm wavelength were performed with several values of air velocity standard deviation to illustrate the effects of air velocity fluctuation on the spectral functions and to attempt to generate functions approximating those shown in Figures 1 and 2. These are illustrated in Figures 3, 4, and 5 for 25 mm hr^{-1} rainfall rate and in Figures 6 and 7 for 2.5 mm hr^{-1} rainfall rate. The spectra and power ratios computed with $\Sigma = 0.05$ and 0.1 show variations which are probably artifacts of the linear interpolation of the scattering coefficients, especially between 5 and 6 m sec^{-1} Doppler velocity. In this velocity region, the scattering characteristics change rapidly with Doppler velocity, since the raindrops producing these effects are falling within 70% to 85% of the maximum raindrop fall speed and the Doppler fall speed is changing slowly with drop size.

The effects of the numerical procedure with small values of Σ are more strikingly illustrated in the cross-spectral amplitude ratio (CSAR) shown in Figures 5a and 7a. Because of the rapid variation of drop size with fall speed for drops of 4 to 5 mm diameter, the full rotation of the amplitude ratio shown in Figure 1 could only be duplicated if the spectral functions were computed at much smaller velocity intervals with correspondingly smaller values of Σ and with non-linear interpolation of the scattering coefficients. The fact that this rapid rotation of the amplitude ratio vector occurs at lower doppler velocities than would be expected from Figure 1 is difficult to explain; this is probably related to the weighting of the cross-spectrum by the backscatter cross-section and size distribution functions and to the irregularities of the cross-section functions resulting from the linear interpolation. At large drop sizes the amplitude ratio varies less rapidly with drop size, and the nature of the computed CSAR near 6 m sec^{-1} Doppler velocity in Figures 5a and 7a is generally preserved with higher values of Σ, although it appears at higher Doppler velocities. The combined effect of the cross-spectral peak (at 4.5 m sec^{-1} Doppler velocity for R 25 mm hr^{-1}) and the portion of the amplitude ratio curve for the largest drops, both of which lie in the upper left quadrant of the complex plane, is to shift the curve of the CSAR into this quadrant with increasing Σ and leave only a relative maximum of the real part of the CSAR as a remnant of the rotation shown in Figure 1. This effect is evident, for example, in Figure 5c for $\Sigma = 0.5$ m sec^{-1} and Figures 5e and 7e for $\Sigma = 1.0$ m sec^{-1}. As Σ increases and the cross-spectral characteristics are spread in the Doppler velocity domain, the relative maximum appears at progressively higher Doppler velocities. Table 2 documents this effect and illustrates the uncertainty of associating the Doppler

velocity at this maximum with a particular drop size, that is, 4.2 mm, based on Figure 1. Such an association of a particular Doppler velocity with a Doppler fall speed component would be a key to extracting the Doppler component due to air velocity.

Table 2. Doppler Velocity (m sec^{-1}) at Maximum of Real Part of Cross-Spectral Amplitude Ratio, for 8.6 mm Wavelength and 40° Elevation Angle

R	Σ (m sec^{-1})			
(mm hr^{-1})	0.05	0.10	0.5	1.0
2.5	5.6	5.7	7.2	12.3
25	5.6	5.6	6.2	8.7

An alternate approach to the problem of separating Doppler components due to fall speed and air velocity is to find a Doppler velocity at which the spectral power ratio (SPR) or the CSAR does not change with Σ. The particular value of the SPR is its asymptotic value, namely, the CDR. (A comparable procedure cannot be applied to the CSAR if appreciable differential phase shift in scattering is present, since the asymptotic value of the CSAR, that is, the CCAR, does not generally lie on the curve defined by the CSAR.) The Doppler velocities at which the computed SPR is equal to the CDR are shown in Table 3. Comparing these values to those in Table 1 we find that they are within ± 0.1 m sec^{-1} of the Doppler mean velocity $\bar{v}_2$ for each rainfall rate. They are 0.2 to 0.3 m sec^{-1} less than the Doppler velocities of the peaks of the power spectra S_2. If one takes the CDR as equal to the power ratio of an individual drop, then the CDRs of -28.80 and -27.50 dB imply drops of 1.8 and 2.1 mm diameter, with Doppler fall speeds of 3.87 and 4.27 m sec^{-1}, respectively. The difference of these values and the respective $\bar{v}_2$ is the estimate of Doppler air velocity, which is zero in this simulation. Further computations will determine the accuracy with which this technique can be applied at different rainfall rates. Since both the CDR and $\bar{v}_2$ are ratios of integrated spectral functions, neither is affected by variations in N_o, the coefficient of the exponential drop size distribution. Deviations from this assumed distribution may affect the results, as will variations in average drop shape due to oscillation. Recent research by Beard et al[13] indicates that the mean axial ratios of oscillating drops are larger than the equilibrium values derived by Pruppacher and Pitter,[9] which in turn are larger than the values

13. Beard, K.V., Johnson, D.B., and Jameson, A.R. (1983) Collisional forcing of raindrop oscillations, J. Atmos. Sci. 40:455-462.

derived by Spilhaus,[8] which were used by Oguchi and Hosoya[7] and in the present model. As detailed quantitative results of the drop oscillation studies become available, it should be possible to revise the spectral model accordingly.

Table 3. Doppler Velocity (m sec^{-1}) at Which Spectral Power Ratio Equals Circular Depolarization Ratio, for 8.6 mm Wavelength and 40° Elevation Angle

R	Σ (m sec^{-1}			
(mm hr^{-1})	0.05	0.10	0.5	1.0
2.5	3.8	3.8	3.7	3.6
25	4.3	4.3	4.2	4.2

3.2 Propagation Effects

The effect of propagation through rain is to change the relative magnitude of the signal in the transmission channel by a component which has a range-dependent phase and amplitude relation to the signal in the opposite channel. This effect is most distinct in the cross-spectral amplitude ratio, which is displaced in the complex plane by an amount equal to the propagation term $2pe^{j\chi}$. Examples of the spectral power ratio and the cross-spectral amplitude ratio in the presence of propagation effects are shown in Figures 8, 9, 10, and 11. (These figures also illustrate effects of noise, to be discussed below.) The determination of the propagation term in the received signals is of importance in that it permits a characterization of the propagation medium, either as a whole or between range samples, and permits the detailed quantitative interpretation of backscatter phenomena in signals that are "contaminated" by propagation effects.

At 8.6 mm wavelength the SPR is not usable for this purpose, since one does not know a priori the relative phase angles of the backscatter and propagation terms, that is, δ and χ. (The case at 10 cm wavelength is simpler, since $\delta \cong \pi$ and $\chi \cong \pi/2$.) Therefore the propagation term must be deduced from the CSAR. In principle, one can take the value of the CSAR at the lowest Doppler velocity as an estimate of the propagation term, on the assumption that the propagation term dominates the backscatter term in that region. This method yields an imprecise result in the presence of noise, since the backscatter amplitude ratio does not reach zero magnitude within the domain of detection of the power spectrum S_2. Thus one must establish a minimum velocity (v_{min}) for the detectability of the spectrum S_2 at which one takes the value of the CSAR as the estimate of the propagation term $2pe^{j\chi}$. From Figures 9 and 11 one can see that the most consistent estimate of the

propagation term can be obtained from the value of the CSAR at the point where the real part is a maximum near the lower end of the Doppler velocity domain. Using a fixed radar noise level, as in Figures 9a and 11a, one finds that this point on the curve corresponds to a value of S_2 approximately 10 dB above the noise level. At 25 mm hr^{-1} rainfall rate and with a radar noise level 50 dB below the peak of S_2, as in Figure 9a, $v_{min} \tilde{=} -0.2$ m sec^{-1}; with a radar noise level 40 dB below the peak of S_2, $v_{min} \tilde{=} 0.5$ m sec^{-1}. Values of CSAR at the minimum velocity for detectability with -40 dB radar noise are tabulated in Table 4, where they can be compared to the corresponding values of the propagation term. The estimates of the propagation term have an absolute error of about 0.0075 independent of range for R = 2.5 mm hr^{-1}, but more than 0.01 and increasing with range at R = 25 mm hr^{-1}. The error for the case R = 2.5 mm hr^{-1} corresponds to one-way differential attenuation and phase shift of 0.065 dB and 0.038 deg. While these may be acceptably small for some purposes, they can introduce unacceptably large error in the resulting estimate of the scattering term $\rho_\alpha \bar{F}(v) e^{j\bar{\delta}(v)}$. Comparison of calculations of the CSAR for various propagation scenarios shows that for d > 1.5 km at 2.5 mm hr^{-1} and for d > 0.2 km at 25 mm hr^{-1} the "corrected" CSAR is a better approximation to the propagation-free CSAR than is the "uncorrected" CSAR. In other words, the correction of the CSAR for propagation effects is best when the error of estimating the propagation term is less than the propagation coefficient 2p. Further analysis will be required to determine the implications of these results for the derivation of the "corrected" SPR as an estimate of the propagation-free SPR, the fraction of oriented scatterers ρ_α, and other backscatter parameters

Use of the method described with empirical data should yield results comparable to those shown above for observations of a backscattering medium in which the smallest scatterers are spherical. In general, if the magnitude of the propagation-free CSAR were zero in any Doppler velocity band, due to the presence of either spherical scatterers or randomly oriented scatterers, one could use the actual value of the CSAR there as a measure of the propagation term. In such a case, however, one would need an independent determination of such a feature in the propagation-free CSAR, perhaps by an observation at very close range. Such an observation might be obtained, for example, in snow but not in a "bright band" situation. In snow, however, one could not be sure that the physical parameters deduced near the ground would be representative of those at higher altitude.

Table 4. Lower Doppler Velocity Limit of Detection of Power Spectrum S_2 With -40 dB Noise Level and Corresponding Value of Cross-Spectral Amplitude Ratio (CSAR), for 8.6 mm Wavelength and 40° Elevation Angle

R (mm hr^{-1})	d (km)	v_{min} (m sec^{-1})	CSAR(v_{min})	$2pe^{jX}$
2.5	0	-0.2	-0.00751 + j 0.00067	0
	0.5		-0.00513 + j 0.00307	0.00265 + j 0.00267
	1.0		-0.00276 + j 0.00546	0.00530 + j 0.00534
	2.0		0.00199 + j 0.0103	0.0106 + j 0.0107
25	0	0.5	-0.0106 + j 0.00122	0
	0.5		0.0219 + j 0.0120	0.0355 + j 0.0118
	1.0		0.0545 + j 0.0228	0.0709 + j 0.0235

3.3 Noise

Effects of radar system noise on the spectral power ratio are shown in Figures 4 and 6. In the presence of such noise, the SPR is an accurate representation of its noise-free form only in the velocity region in which the power spectrum in the transmission channel, S_1, is more than about 10 dB above the noise level. Thus, for the cases illustrated here, the SPR is of little value if the radar noise level were higher than about 50 dB below the peak of S_2. Because the radar system noise is assumed to be uncorrelated between the two polarization channels, it does not affect the cross-spectrum, and the CSAR is therefore definable across the entire Doppler domain within which S_2 is above the noise level. Radar noise effects can be seen by comparing Figures 5c and 5d, Figures 5e and 5f, Figures 7c and 7d, and Figures 7e and 7f. It appears that in the presence of radar noise the CSAR is a more useful function for analysis than is the SPR. For example, although the relative maximum of the real part is lost when $\Sigma = 1.0$ and the radar noise level is at -50 dB (for example, Figure 5f), the form of the function is preserved accurately for Doppler velocities up to about 8 m sec^{-1}. The quantitative details of the CSAR are, of course, dependent on the orientation parameter ρ_α.

If one simulates the noise as being due to spectral leakage, as described in Section 2, then the SPR and CSAR approach values of $S_{1\,max}/S_{2\,max}$ and $S_{12\,max}/S_{2\,max}$ at the extremes of the Doppler velocity domain. These effects are illustrated in Figures 8b and 10b for the SPR and Figures 9b and 11b for the CSAR. This simulation permits the definition of S_1 and, hence, the SPR over a wider velocity domain than in the case of simulated radar noise described above. Because the spectral noise affects the cross-spectrum, the CSAR is definable over a narrower velocity domain than in the case of simulated radar noise.

In practice, one will be interested in situations for which the CDR is as low as 10^{-3}, that is, -30 dB, assuming that the radar antenna permits such measurements. In order to have useful signal in the transmission channel, S_1 must be more than 10 dB above the radar noise level within an appreciable velocity domain. The spectrum in the opposite channel, having a peak value of about 30 dB higher than the peak of S_1, will be more than 40 dB above the radar noise level within a similar velocity domain. Since common data windows used in conjunction with fast Fourier transforms for spectral estimation will suppress spectral leakage to about 40 or 45 dB in frequency side lobes, the domain of the power spectrum S_2 will generally be limited by spectral noise rather than by radar system noise. If the spectrum S_1 were also limited by spectral noise at the 40 dB level, then the radar noise level would have to be more than 70 dB below the peak of S_2, implying the possibility of receiver saturation in the channel opposite to the transmission channel. Hence S_1 is most likely to be limited by radar system noise. If the radar is designed with high isolation between channels, then the cross-spectrum will always be limited by spectral leakage noise.

3.4 Rayleigh Scattering

Calculations analogous to the foregoing, but for a wavelength of 1.5 cm, are illustrated in Figures 12-16. At this wavelength the scattering differential phase shift δ is near π for equivalent drop diameters of 4 mm and less. These sizes generally dominate the computed spectral functions, especially for moderate values of Σ, so that the scattering term in the cross-spectral amplitude ratio is predominantly real. Attenuation and differential attenuation are small, so that the propagation term $2p e^{j\chi}$ is due almost entirely to differential phase shift. The angle χ ranges from $0.48\,\pi$ (86.8°) to 0.49π (88.2°) for rainfall rates of 150 to 0.25 mm hr^{-1}. At 25 mm hr^{-1} rainfall rate and 40° elevation angle with $\Sigma = 0.5$ m sec^{-1} (Figure 14b) the angle δ lies between 179.5° and -174.3° across the velocity interval 0.3 to 7.7 m sec^{-1}, where the spectrum S_2 is more than 5 dB above a -40 dB radar noise level.

If the real part of the CSAR is interpreted as due to scattering and the imaginary part due to propagation, the error of estimating the propagation term will be given by the quantity $[Re^2(2pe^{j\chi}) + Im^2(\varphi_\alpha \bar{\nu}(v_{min}) e^{j\delta(v_{min})})]^{1/2}$. At a propagation distance of 2 km through heavy (25 mm hr^{-1}) rain, illustrated in Figure 16, the magnitude of error is about 0.0016, due largely to the imaginary part of the scattering term. The simpler relationship of the scattering and propagation terms at the longer wavelength should facilitate the identification of non-Rayleigh scatterers and the presence of non-zero canting angles in the scattering and propagation media.

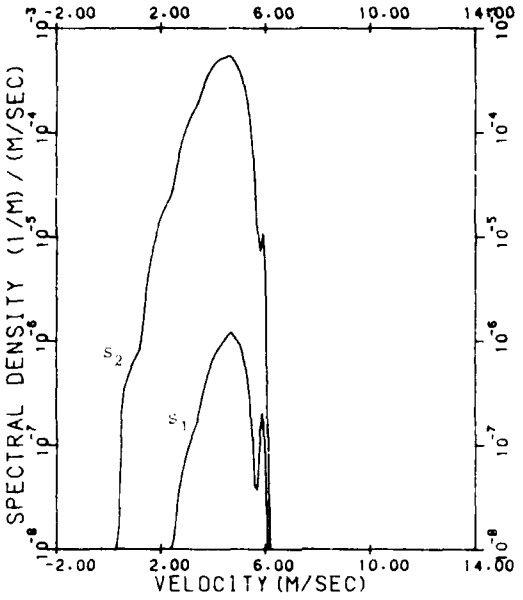

Figure 3a. Power spectra of signals in the transmission (1) and orthogonal (2) channels of a circularly polarized 8.6 mm wavelength radar at 40° elevation angle in 25 mm hr^{-1} rain with Σ = 0.05 m sec^{-1}.

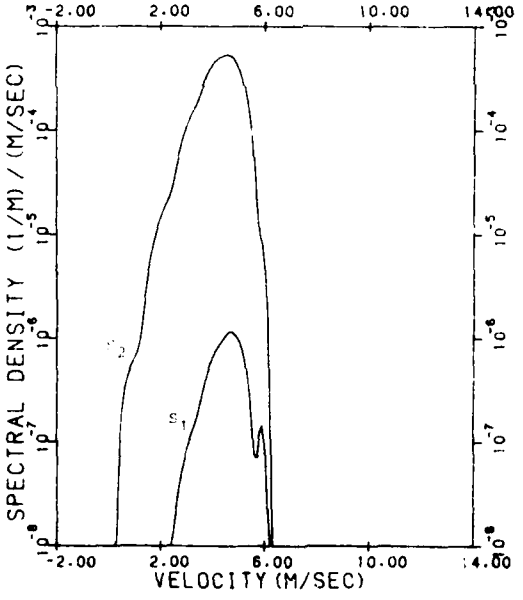

Figure 3b. Same as Figure 3a but with Σ = 0.1 m sec^{-1}.

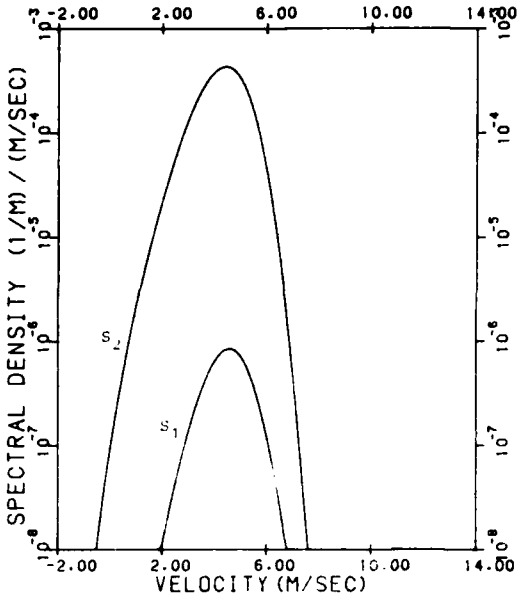

Figure 3c. Same as Figure 3a but with Σ = 0.5 m sec^{-1}.

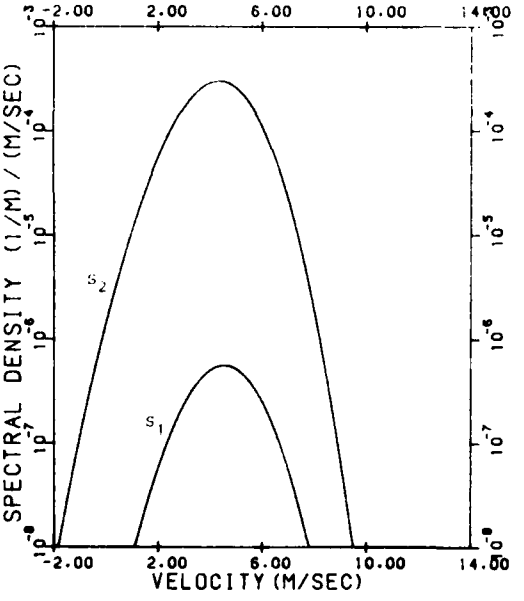

Figure 3d. Same as Figure 3a but with Σ = 1.0 m sec^{-1}.

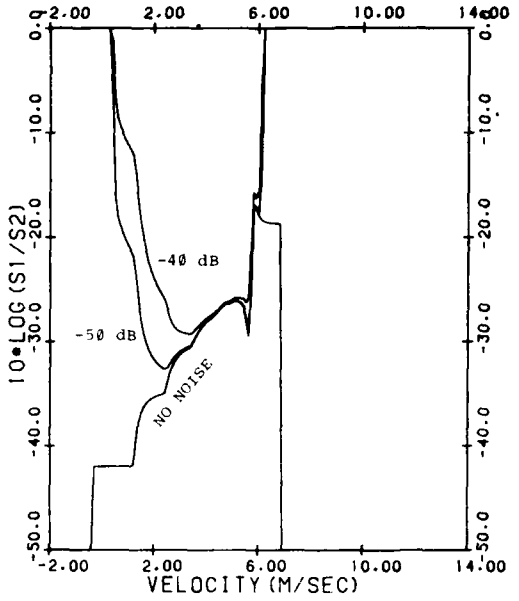

Figure 4a. Spectral power ratio for 40° elevation angle in 25 mm hr^{-1} rain with $\Sigma = 0.05$ m sec^{-1} with no noise and with radar noise levels of 50 and 40 dB below the peak value of S_2. Apparent cutoffs of the noise-free case near -1.5 and 7 m sec^{-1} Doppler velocity are due to numerical limits of the computations. In the presence of noise the power ratio provides an estimate of the noise-free function over a limited velocity domain.

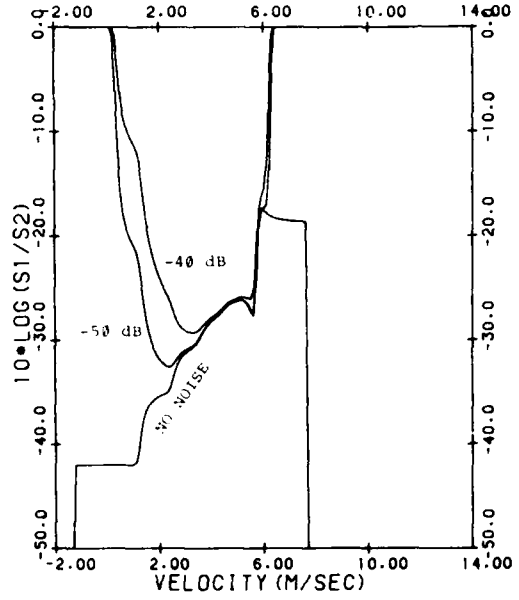

Figure 4b. Same as Figure 4a but with $\Sigma = 0.1$ m sec^{-1}.

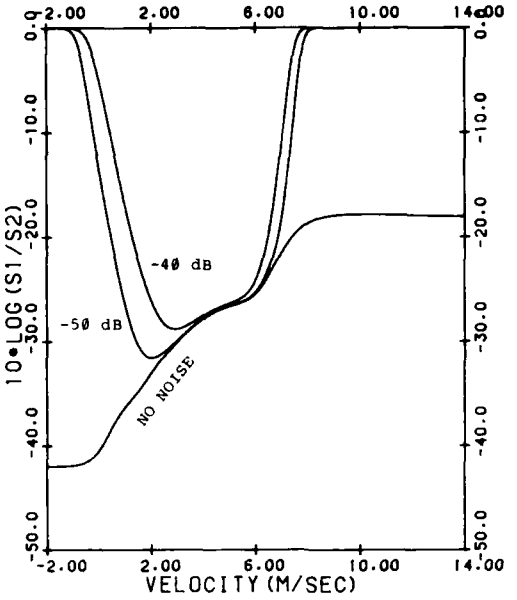

Figure 4c. Same as Figure 4a but with $\Sigma = 0.5$ m sec^{-1}.

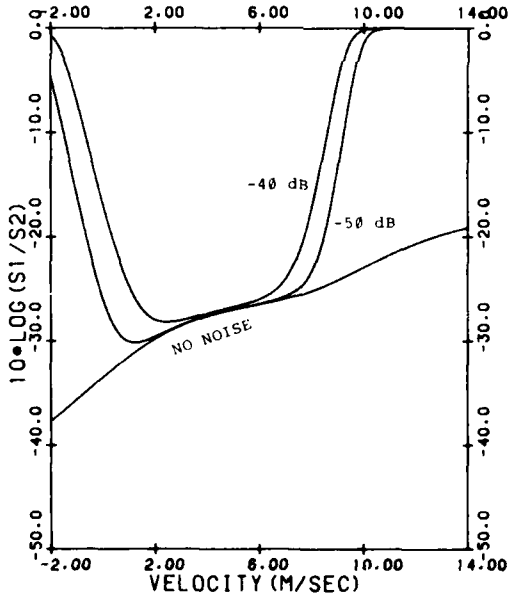

Figure 4d. Same as Figure 4a but with $\Sigma = 1.0$ m sec^{-1}.

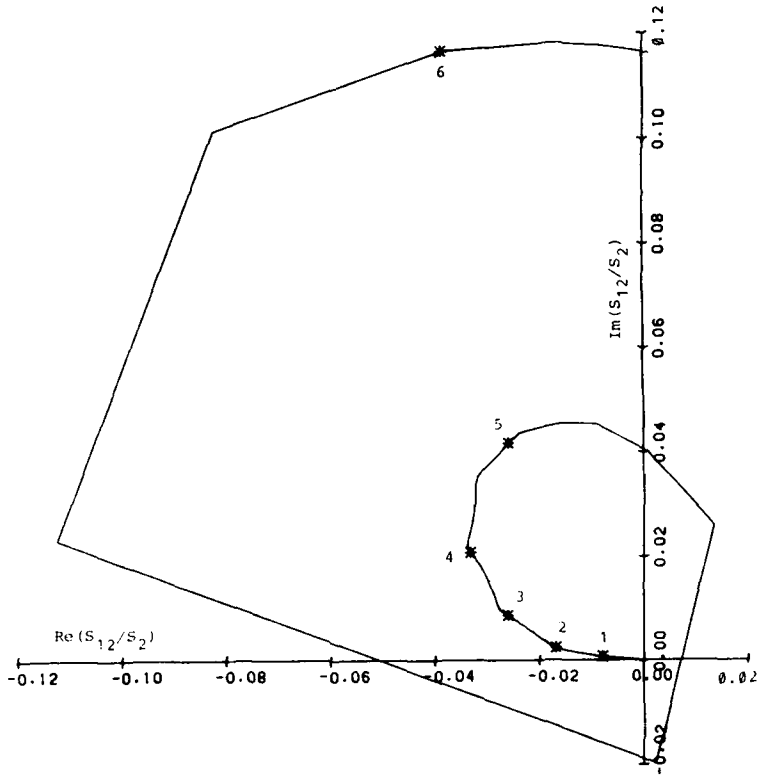

Figure 5a. Cross-spectral amplitude ratio for 40° elevation angle in 25 mm hr^{-1} rain with Σ= 0.05 m sec^{-1} and no noise. Segmented appearance of function beyond about 5.5 m sec^{-1} Doppler velocity is due to rapid variation of drop size and shape with Doppler fall speed in this region.

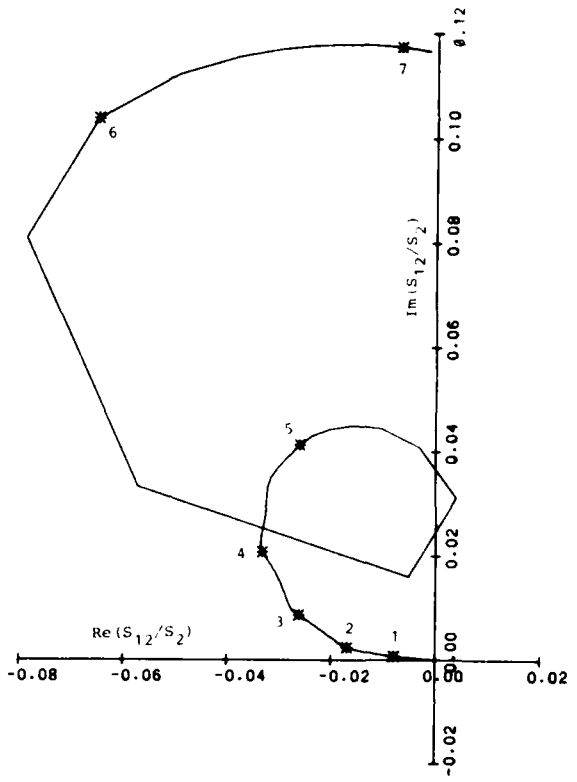

Figure 5b. Same as Figure 5a but with $\Sigma = 0.1$ m sec^{-1}.

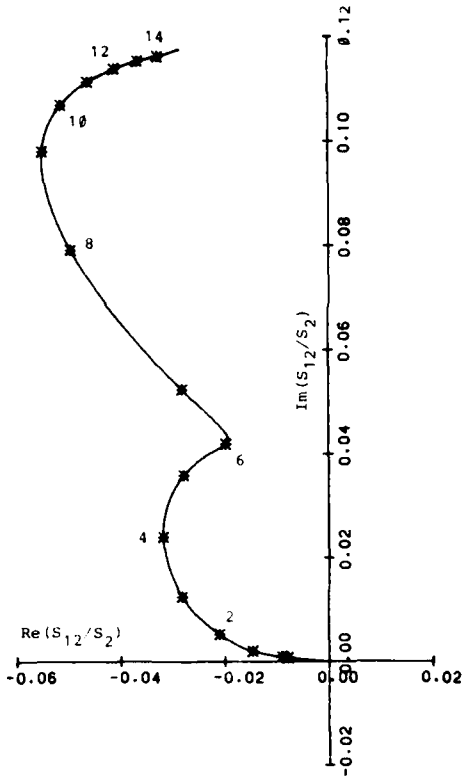

Figure 5c. Same as Figure 5a but with $\Sigma = 0.5$ m sec^{-1} Smoothing due to increasing width of velocity weighting function is evident.

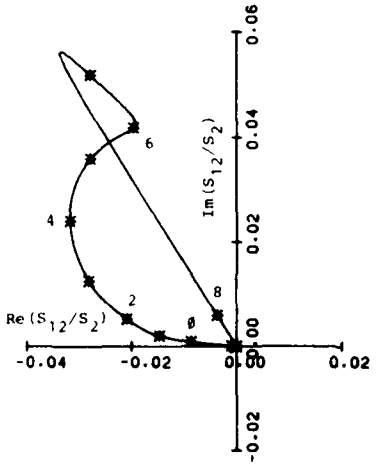

Figure 5d. Same as Figure 5c but with radar noise level of 50 dB below the peak value of S_2.

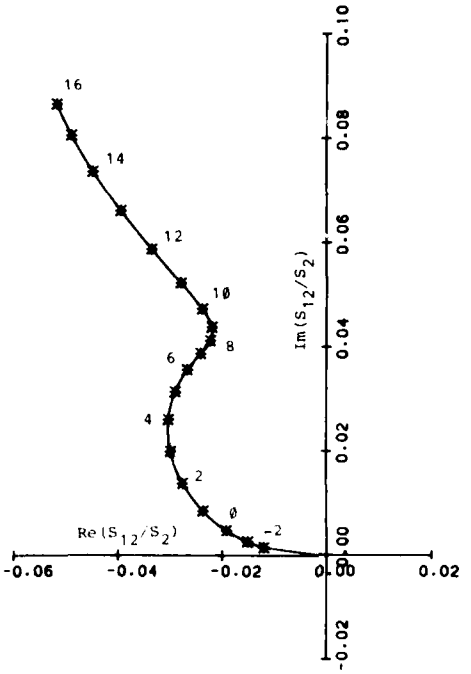

Figure 5e. Same as Figure 5a but with $\Sigma = 1.0$ m sec^{-1}.

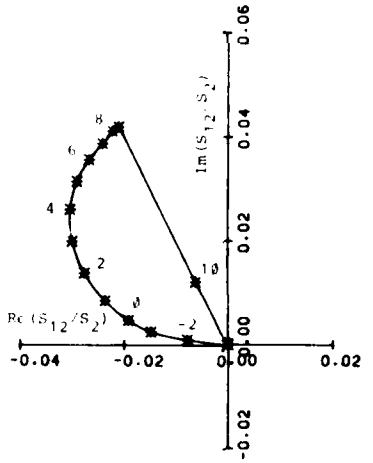

Figure 5f. Same as Figure 5e but with radar noise level of 50 dB below the peak value of S_2. Maximum of the real part near 9 m sec^{-1} is not discernable in this case.

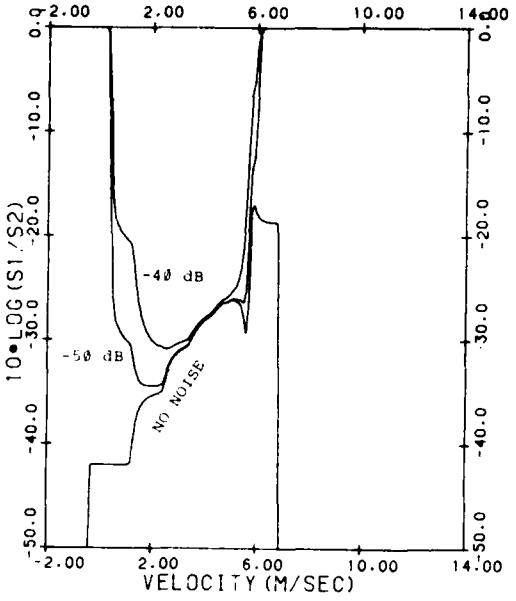

Figure 6a. Spectral power ratio for 40° elevation angle in 2.5 mm hr^{-1} rain with $\Sigma = 0.05$ m sec^{-1} with no noise and with noise levels of 50 and 40 dB below the peak value of S_2.

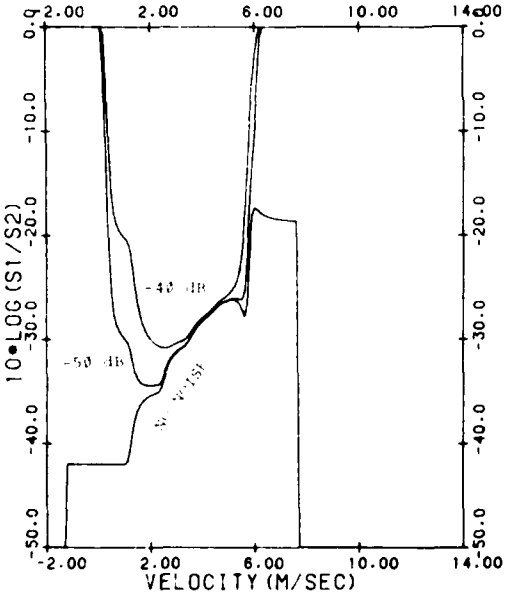

Figure 6b. Same as Figure 6a but with $\Sigma = 0.1$ m sec^{-1}.

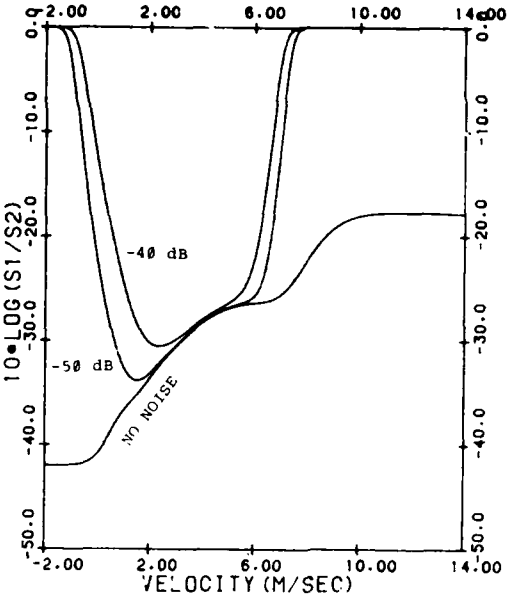

Figure 6c. Same as Figure 6a but with Σ = 0.5 m sec^{-1}.

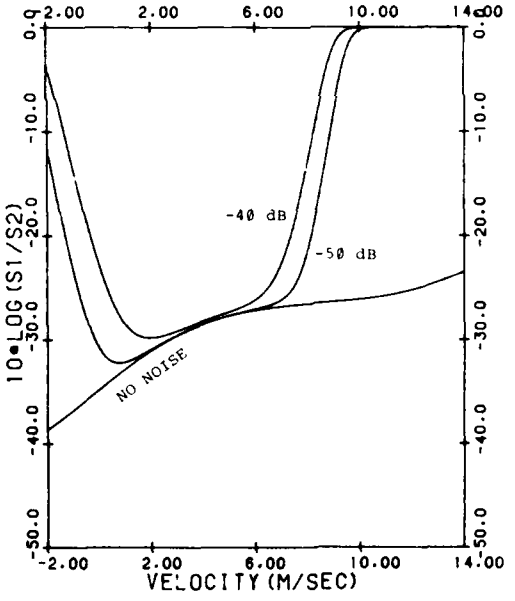

Figure 6d. Same as Figure 6a but with Σ = 1.0 m sec^{-1}.

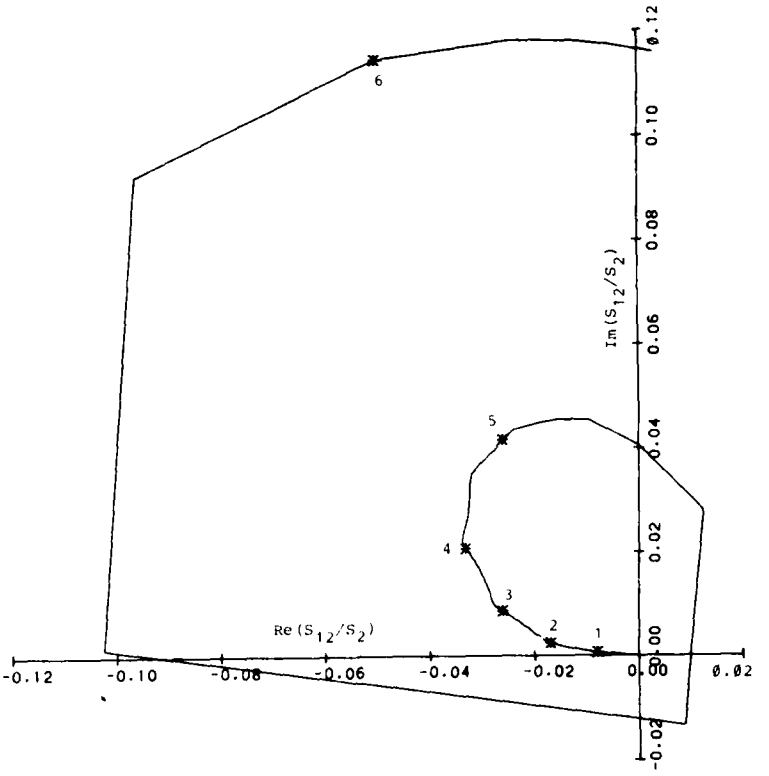

Figure 7a. Cross-spectral amplitude ratio for 40° elevation angle in 2.5 mm hr^{-1} rain with $\Sigma = 0.05$ m sec^{-1} and no noise.

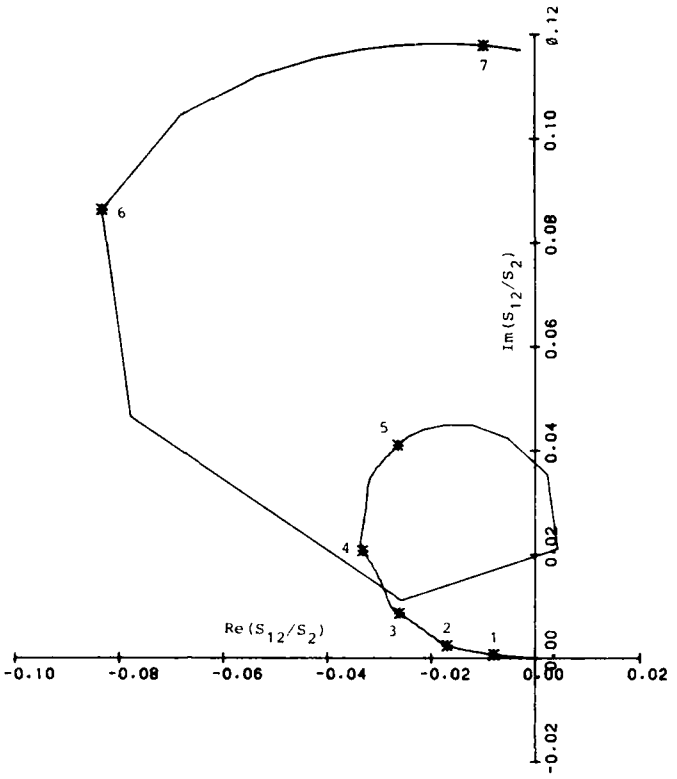

Figure 7b. Same as Figure 7a but with Σ = 0.1 m sec^{-1}.

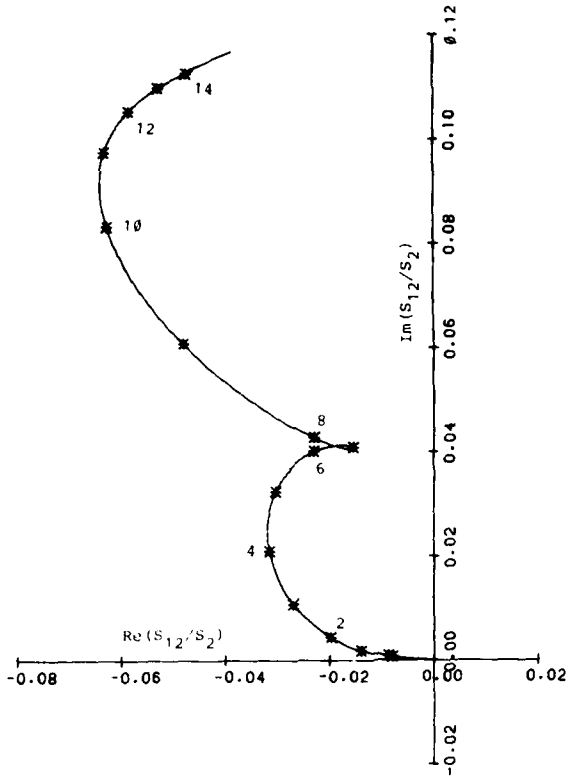

Figure 7c. Same as Figure 7a but with $\Sigma = 0.5$ m sec^{-1}.

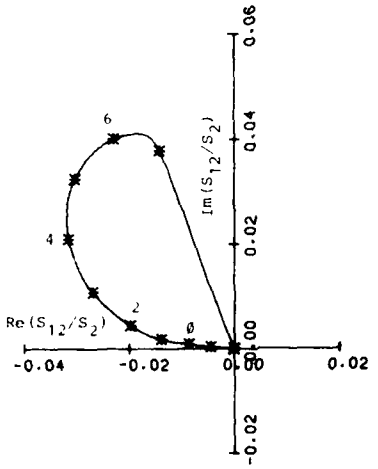

Figure 7d. Same as Figure 7c but with radar noise level of 50 dB below the peak value of S_2. Disappearance of the relative maximum of the real part near 7 m sec^{-1} is due to the narrower Doppler velocity domain of the spectral functions at this rainfall rate compared to those at 25 mm hr^{-1}. Compare this figure to Figure 5d.

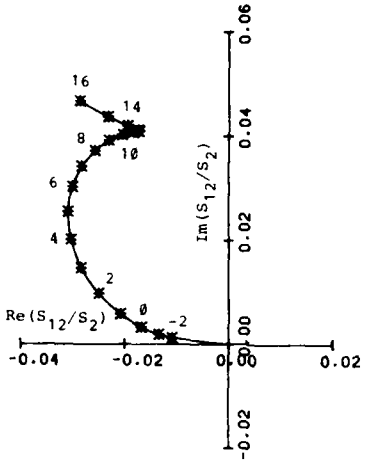

Figure 7e. Same as Figure 7a but with $\Sigma = 1.0$ m sec^{-1}

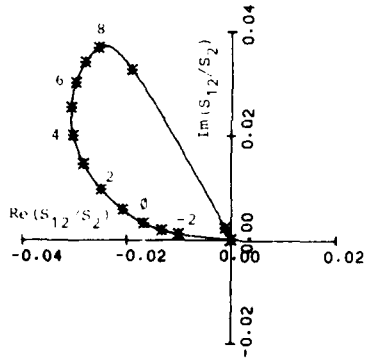

Figure 7f. Same as Figure 7e but with noise level of 50 dB below the peak value of S_2

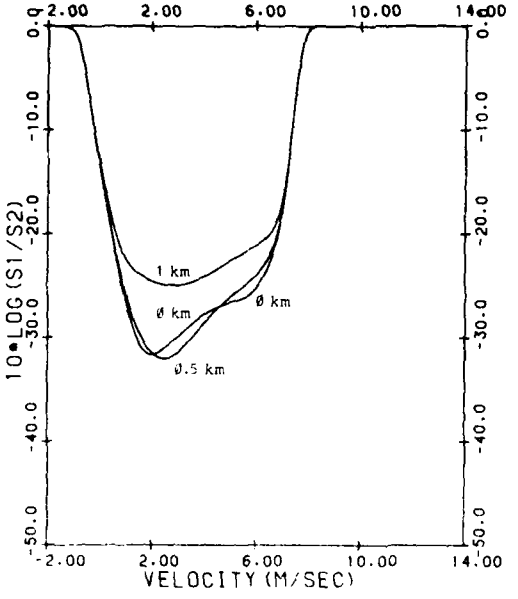

Figure 8a. Spectral power ratio for 40° elevation angle in 25 mm hr^{-1} rain with Σ = 0.5 m sec^{-1}, radar noise level of 50 dB below the peak value of S_2, and propagation distances of 0, 0.5, and 1 km. Changes with distance are due to the relative magnitudes and phases of the backscattering and propagation terms.

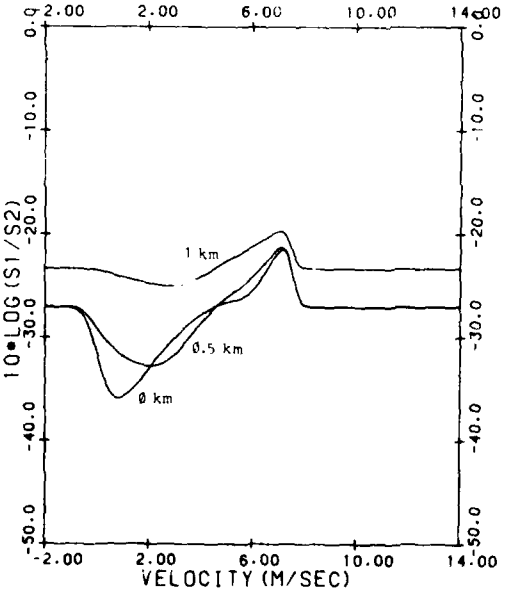

Figure 8b. Same as Figure 8a with no radar noise but with spectral noise in each spectrum at 40 dB below the respective peak value. Useful domain of the function is increased relative to that in the presence of radar noise.

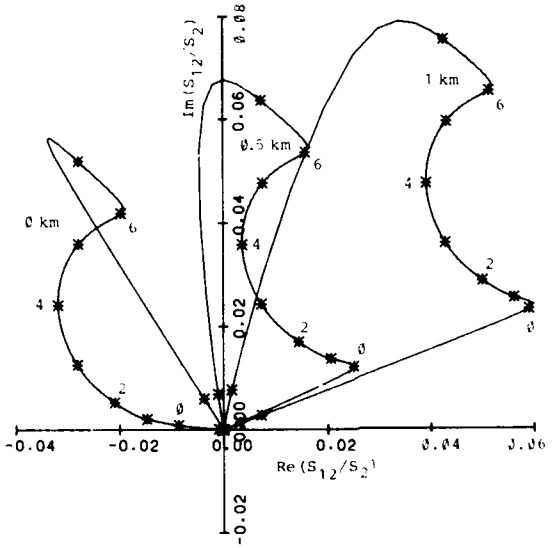

Figure 9a. Cross-spectral amplitude ratio for 40° elevation angle in 25 mm hr^{-1} rain with Σ = 0.5 m sec^{-1}, radar noise level of 50 dB below the peak value of S_2 and propagation distances of 0, 0.5, and 1 km. Since ρ_α = 1, the squared magnitude of this function is approximately equal to the spectral power ratio shown in Figure 8a for the same values of propagation distance.

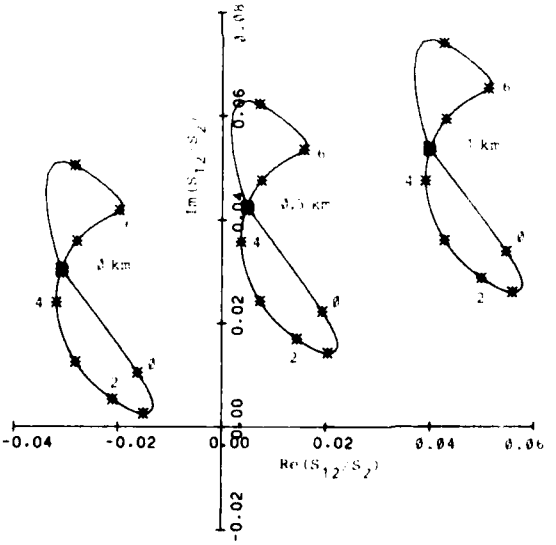

Figure 9b. Same as Figure 9a with no radar noise but with spectral noise at 40 dB below the peak values of S_{12} and of S_2. Compare this figure with Figure 8b.

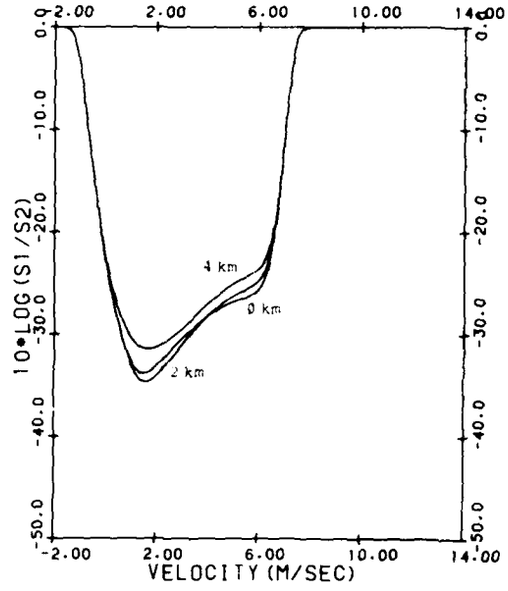

Figure 10a. Spectral power ratio for 40° elevation angle in 2.5 mm hr^{-1} rain with $\Sigma = 0.5$ m sec^{-1}, radar noise level of 50 dB below the peak value of S_2, and propagation distances of 0, 2, and 4 km.

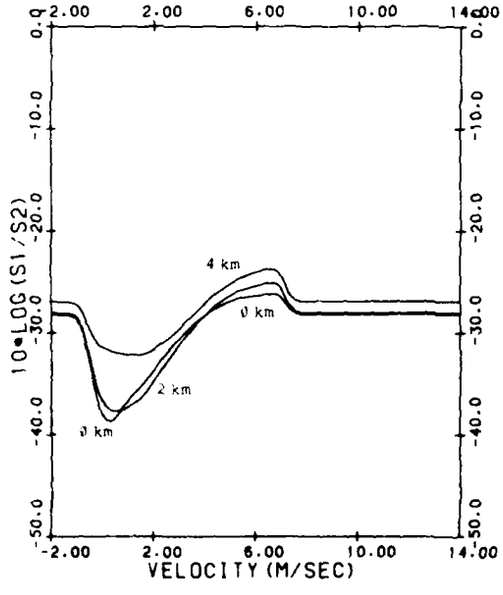

Figure 10b. Same as Figure 10a with no radar noise but with spectral noise in each spectrum at 40 dB below the respective peak value.

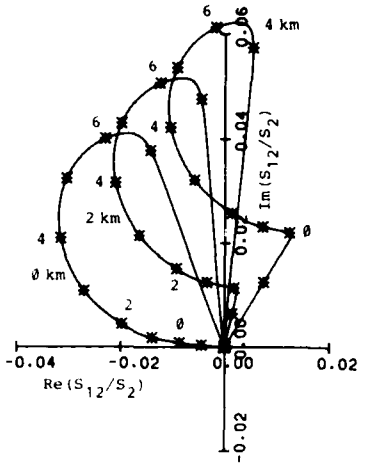

Figure 11a. Cross-spectral amplitude ratio for 40° elevation angle in 2.5 mm hr^{-1} rain with $\Sigma = 0.5$ m sec^{-1}, radar noise level of 50 dB below the peak value of S_2, and propagation distances of 0, 2, and 4 km. Compare this figure to Figure 10a to see the roles of the relative magnitude and phase of the backscattering and propagation terms in defining the range-wise changes of the spectral power ratio.

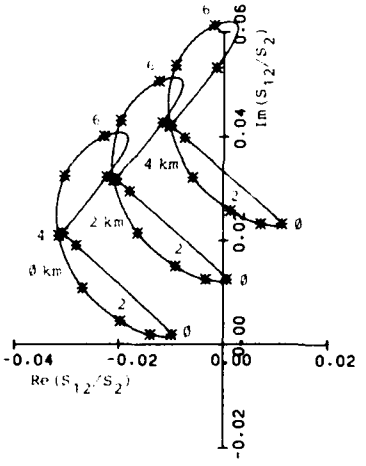

Figure 11b. Same as Figure 11a with no radar noise but with spectral noise at 40 dB below the peak values of S_{12} and S_2. Compare this figure to Figure 10b.

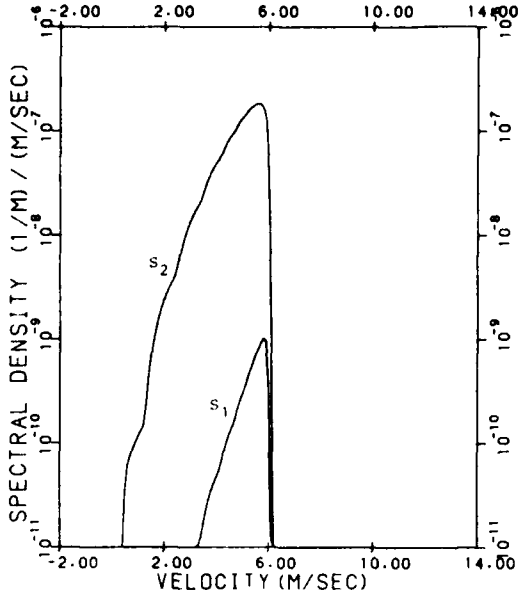

Figure 12a. Power spectra of signals in the transmission (1) and orthogonal (2) channels of a circularly polarized 7.5 cm wavelength radar at 40° elevation angle in 25 mm hr^{-1} rain with $\Sigma = 0.05$ m sec^{-1}. Compare this figure to Figure 3a, which illustrates non-Rayleigh scattering with identical values of all parameters except the wavelength.

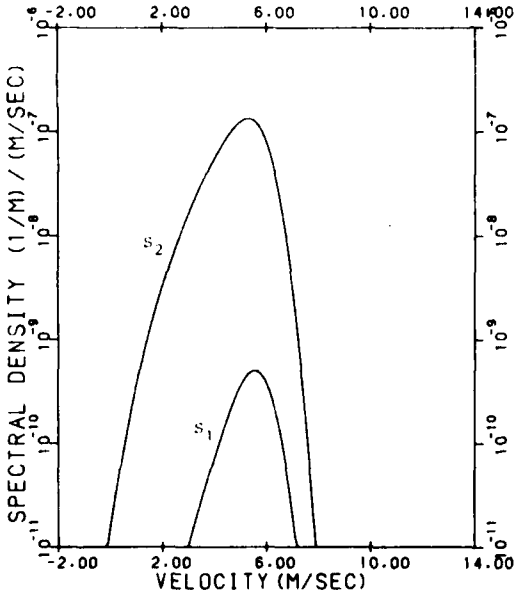

Figure 12b. Same as Figure 12a but with $\Sigma = 0.5$ m sec^{-1}.

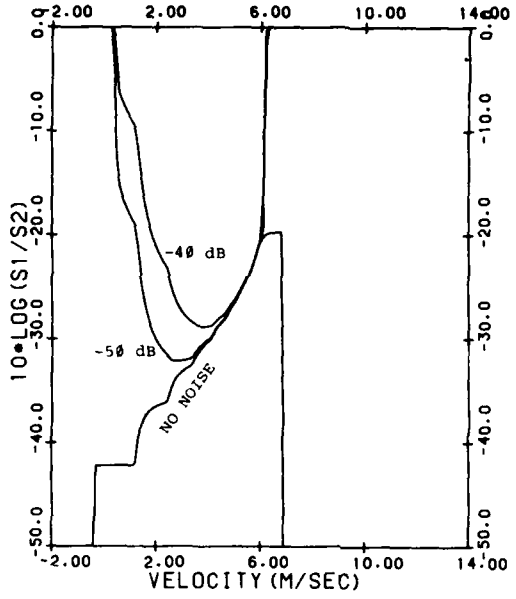

Figure 13a. Spectral power ratio for 7.5 cm wavelength and 40° elevation angle in 25 mm hr^{-1} rain with Σ = 0.05 sec^{-1} with no noise and with radar noise levels of 50 and 40 dB below the peak value of S_2.

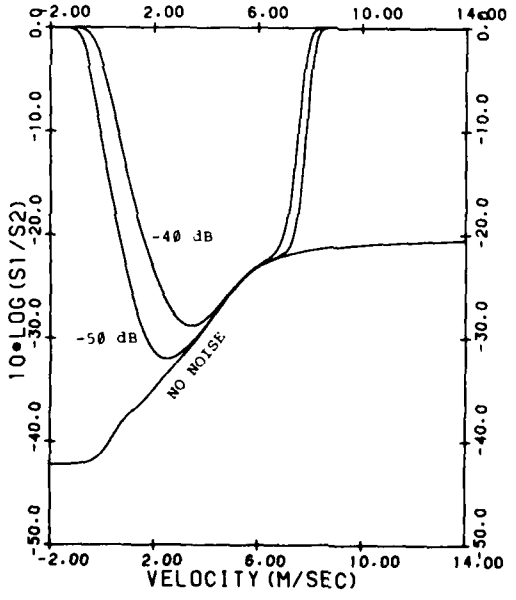

Figure 13b. Same as Figure 13a but with Σ = 0.5 m sec^{-1}.

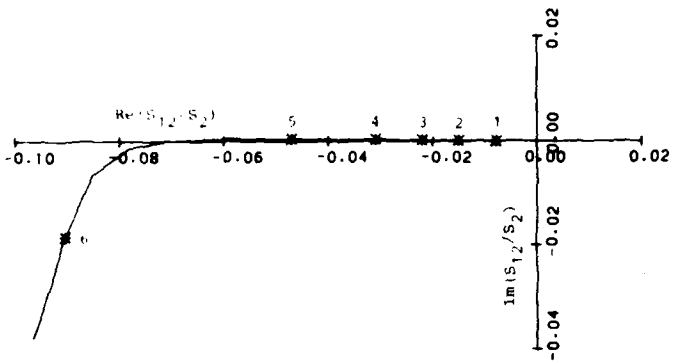

Figure 14a. Cross-spectral amplitude ratio for 7.5 cm wavelength and 40° elevation angle in 25 mm hr^{-1} rain with Σ = 0.05 m sec^{-1} and no noise. Divergence of function from negative real axis beyond about 5.7 m sec^{-1} Doppler velocity is due to non-Rayleigh scattering effects.

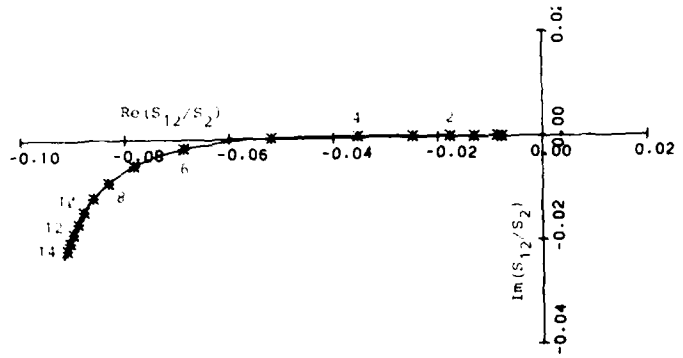

Figure 14b. Same as Figure 14a but with Σ = 0.5 m sec^{-1}.

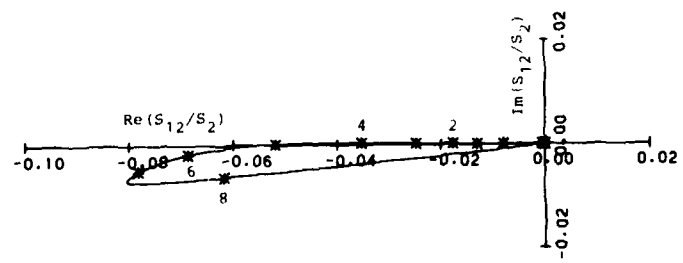

Figure 14c. Same as Figure 14b but with radar noise level of 50 dB below the peak value of S_2. Effect of noise is to obscure most of the non-Rayleigh scattering component above 7 m sec^{-1} Doppler velocity.

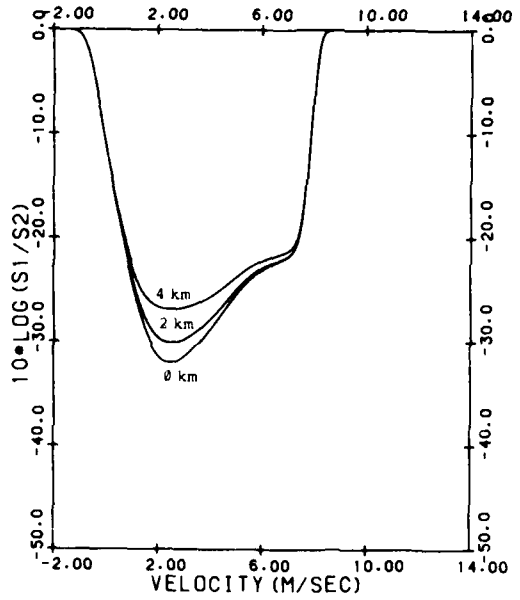

Figure 15a. Spectral power ratio for 7.5 cm wavelength and 40° elevation angle in 25 mm hr^{-1} rain with $\Sigma = 0.5$ m sec^{-1}, radar noise level of 50 dB below the peak value of S_2, and propagation distances of 0, 2, and 4 km. The function increases monotonically with distance because the backscattering and propagation terms differ in phase by approximately 90°.

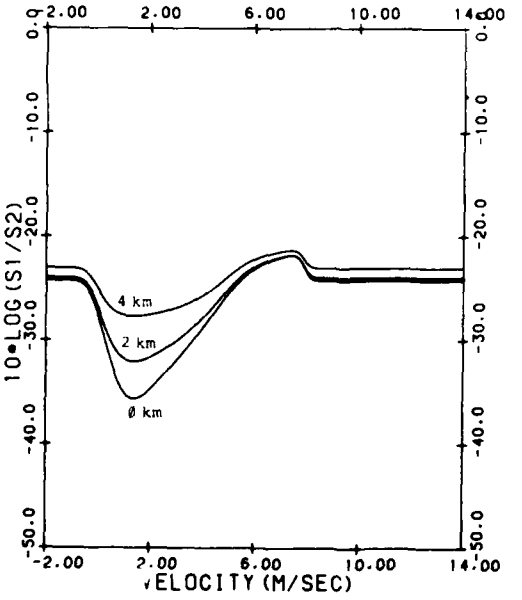

Figure 15b. Same as Figure 15a with no radar noise but with spectral noise in each spectrum at 40 dB below the respective peak value.

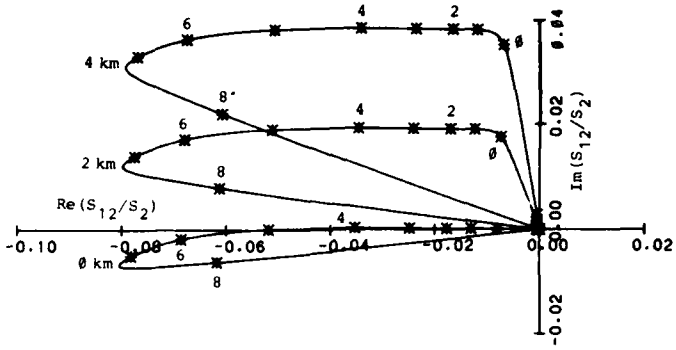

Figure 16a. Cross-spectral amplitude ratio for 7.5 cm wavelength and 40° elevation angle in 25 mm hr^{-1} rain with Σ = 0.5 m sec^{-1}, radar noise level of 50 dB below the peak value of S_2, and propagation distances of 0, 2, and 4 km. Imaginary part of this function taken between 1 and 5 m sec^{-1} Doppler velocity yields an excellent approximation of the propagation term, which is due mainly to differential phase shift.

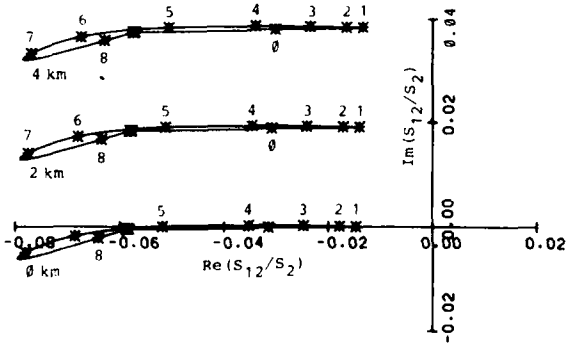

Figure 16b. Same as Figure 16a with no radar noise but with spectral noise at 40 dB below the peak values of S_{12} and S_2.

4. CONCLUSIONS

We have developed a model for simulating spectral functions derivable from a coherent polarization diversity radar transmitting circular polarization and observing backscatter from rain. The spectral functions have been computed for radar wavelengths of 8.6 mm and 7.5 cm and for several values of air velocity variance and propagation distance. We performed these computations for 40° elevation angle, for jointly maximizing the signal amplitude in the transmission channel (proportional to $\cos^2\phi$) and the Doppler velocity variance due to fall speeds (proportional to $\sin^2\phi$).

The results illustrate several requirements that must be met in the analysis of this type of radar data. The spectrum in the transmission channel must be more than 10 dB above the noise level over an appreciable velocity domain in order that the spectral power ratio be useful for analysis. The cross-spectral amplitude ratio appears to have more analytical value because it is not as severely affected by noise. Large values of air velocity variance, for example, approaching $1\ m^2\ sec^{-2}$, limit the usefulness of the spectral functions, as certain features that might be associated with particular drop sizes are thereby shifted in Doppler velocity.

A fairly accurate estimate of the Doppler component of air velocity can be derived at 8.6 mm wavelength by identifying the Doppler fall speed component at $\bar{v}_2$ with drops of size corresponding to the power ratio $S_1(\bar{v}_2)/S_2(\bar{v}_2)$. This estimate is dependent on the size-shape relation assumed in the model, and refinements of the specification of average drop shape will lead to model results more closely applicable to experimental measurements. Use of this procedure in the presence of differential propagation effects will lead to inaccuracies unless the propagation term is estimated accurately. The present model can be extended to permit evaluation of the resulting uncertainties. Calculations at 7.5 cm, although not as comprehensive as at 8.6 mm, indicate that comparable results can be obtained.

Estimation of the total propagation term in the CSAR yields an error of about 0.0075 to 0.010 in magnitude at 8.6 mm wavelength, which may not be acceptable for some purposes. The incremental propagation term, that is, from one range gate to the next, can be evaluated with more accuracy, probably exceeding the accuracy obtainable from the CCAR based on non-coherent radar data. At 7.5 cm wavelength, where the scattering amplitude ratio is predominantly real, the total propagation term can be estimated with much more accuracy than at 8.6 mm.

Several future developments and applications of the model are possible. Further calculations can be made with the existing formulation to evaluate uncertainties of estimating the Doppler air velocity component and the propagation term. The noise simulation options should be combined to more closely match experimental

conditions. A signal component corresponding to radar system cross-polarization could be included. Of greatest scientific interest (and of greatest difficulty) would be the modification of the model to incorporate the newest data on raindrop shapes and to permit the simulation of mixed-phase media.

References

1. Metcalf, J.I., and Echard, J.D. (1978) Coherent polarization-diversity radar techniques in meteorology, J. Atmos. Sci. 35:2010-2019.

2. Metcalf, J.I. (1981) Propagation effects on a coherent polarization-diversity radar, Radio Sci. 16:1373-1383.

3. Metcalf, J.I. (1983) Interpretation of simulated polarization diversity radar spectral functions, Radio Sci. 18:*in press*.

4. Warner, C., and Rogers, R.R. (1977) Polarization-diversity Radar: Two Theoretical Studies, Sci. Rept. MW-90, Stormy Weather Group McGill University, Montreal, Quebec, Canada.

5. Pasqualucci, F., Bartram, B.W., Kropfli, R.A., and Moninger, W.R. (1983) A millimeter-wavelength dual-polarization Doppler radar for cloud and precipitation studies, J. Clim. Appl. Meteor. 22:758-765.

6. Metcalf, J.I., and Matthews, J.E., III (1981) Numerical Simulation of Coherent Polarization-diversity Radar Spectral Functions, Scientific Report No. 1, Natl. Sci. Foundation Grant ATM-8018382, Project A2818, Engr. Expt. Stn., Ga. Inst. of Tech., Atlanta, Georgia.

7. Oguchi, T., and Hosoya, Y. (1974) Scattering properties of oblate raindrops and cross polarization of radio waves due to rain (Part II): Calculations at microwave and millimeter wave regions, J. Radio Res. Labs. (Japan) 21:191-259.

8. Spilhaus, A.F. (1948) Raindrop size, shape, and falling speed, J. Meteor. 5:108-110.

9. Pruppacher, H.R., and Pitter, R.L. (1971) A semi-empirical determination of the shape of cloud and rain drops, J. Atmos. Sci. 28:86-94.

10. Marshall, J.S., and Palmer, W.M. (1948) The distribution of raindrops with size, J. Meteor. 5:165-166.

11. McCormick, G.C., and Hendry, A. (1975) Principles for the radar determination of the polarization properties of precipitation, Radio Sci. 10:421-434.

12. Best, A. C. (1950) Empirical formulae for the terminal velocity of water drops falling through the atmosphere, Quart. J. Roy. Meteor. Soc. 76:302-311.

13. Beard, K. V., Johnson, D. B., and Jameson, A. R. (1983) Collisional forcing of raindrop oscillations, J. Atmos. Sci. 40:455-462.

ferences

r drops
311.
rcing

END

DATE
FILMED

10 — 83

DTIC